4
Interactions of Fluorinated Agrochemicals with Humic Materials

4.1 INTRODUCTION

Natural organic matter (NOM) can be found in soils, sediments, oceans, rivers, lakes, and ponds as it exists ubiquitously in the environment. NOM present in terrestrial region is known as soil organic matter (SOM) while NOM dissolved in aquatic environment is called dissolved organic matter (DOM). NOM is a complex mixture of inhomogeneous chemical components and exists in oligomeric state, and participates in several environmental processes. It plays a vital role in the global carbon cycle being a potentially large reservoir of labile carbon. NOM interacts and modulates the biochemistry of a variety of organic and inorganic pollutants by regulating their transport, bioavailability, toxicity, and degradation within the environment. Consequently, sediments, soils and water bodies act as the major environmental sinks for several anthropogenic compounds [Longstaffe et al., 2010]. Among the various fractions of NOM, humic substances (HS) including humic acid (HA) are the most abundant form of organic carbon and constitute major parts of SOM and DOM. HS are being considered as appropriate proxies of NOM and are used to understand the NOM chemistry and behaviour in environment as per several literature reports [Khalaf et al., 2003; Ohno et al., 2019]. HS possess the ability to sorb and bind various soil pollutants dictating their destiny within the environment [Albers et al., 2008]. Hence, the analysis of the interaction of HS with organic pollutants such as agrochemicals attracts widespread attention among the environmental researchers unravelling the fate of these chemical compounds in soil-water system [Atashgahi et al., 2018; Mazzei and Piccolo, 2015; Nauen et al., 2015; Sahin and Karpuzcu, 2020; Wang et al., 2020]. Studies related to the nature of these interactions can also provide useful insight in designing of suitable remediation processes of these pollutants from aquatic and terrestrial environments [Mazzei and Piccolo, 2015; Simpson and Simpson, 2014].

The term 'agrochemicals' encompasses a broad range of chemicals known as insecticides, fungicides, herbicides, rodenticides, plant growth modifiers, to name a few [Aktar et al., 2009]. The present chapter therefore, brings forth interaction analysis of selected fluorinated agrochemicals in particular with HA extracted from soil samples highlighting two major effects of HA, namely, encapsulation of pollutants and alteration of photo-degradation of organic pollutants using ^{19}F solution-state NMR approaches. The following sections provide brief discussion on the nature of HS, its role in the environment and specific NMR methods used in environmental research.

4.1.1 Structural properties of HS: Possibility of host-guest interaction

The unique structural properties of HS including HA lead to its diverse applications in medicine, agriculture, industry and environmental protection [David et al., 2014]. HS possesses high chemical reactivity due to the presence of several organic functional groups that provide an ample number of binding sites for small molecules to bind [Fang et al., 2015; Guo et al., 2019]. The properties of HS are the resultant of the interactions among the chemical constituents, namely aliphatic, aromatic, carbohydrate, and amino acids containing moieties forming a polydisperse mixture [Khalaf et al., 2003]. The complex structure and formation of HS have always been a topic of debate [Aldmour et al., 2019]. On one hand, the traditional 'polymer model' suggests that HS are large randomly coiled polymeric macromolecules [Ghosh and Schnitzer, 1979; Swift, 1999; Wandruszka, 2000]; while the recent evidences indicate that HS form superstructures due to self-assembling of relatively small heterogeneous molecules mainly

held by hydrophobic dispersive forces [Kögel-Knabner, 2000; Piccolo, 2001; Sutton and Sposito, 2005]. The conceptual models and discussions on HS point out that the inherent amphiphilic nature of HS tends to manifest both intra and inter-molecular aggregation generating micelle like structure with hydrophilic and hydrophobic domains [Fan et al., 2004; Guetzloff and Rice, 1994; Simpson, 2002; Varga et al., 2000; Wandruszka et al., 1997; Zang, et al., 2000]. Due to similarities and differences with conventional surfactant micelles [Engebretson and Wandruszka, 1997; Klavins and Purmalis, 2010; Piccolo et al., 1996], these HS super structures are more preferably referred as pseudo-micelles. HA, the major constituent of HS exhibits similar micelle formation in soil-water systems. Pollutants of proper sizes can be trapped in such micellar HA structure behaving as a host that either store the pollutant or degrade it faster. Depending on their interaction and degradation behavior in presence of HA, these anthropogenic compounds can either leach into groundwater or it may persist onto the surface of the soil over the years [Fan et al., 2004; Guetzloff and Rice, 1994; Kögel-Knabner, 2000; Piccolo, 2001; Saint-Fort and Visser, 1988; Simpson et al., 2002; Sutton and Sposito, 2005; Wandruszka, 1998; Wershaw, 1994; Yen et al., 2000; Zang et al., 2000].

4.1.2 Photo-degradation of agrochemicals by HA

Photo-degradation is one of the most important natural processes determining the distribution of agrochemicals in the soil-water system. Direct and indirect photo-degradation of these organic molecules regulate the bioavailability and elimination of the parent and degraded residues in soil [Guo et al., 2000]. The rate of degradation depends on various factors such as exposure to sunlight, variation of pH, the activity of soil microorganism, presence of inorganic and metal ions (NO_3^-, NO_2^-, Fe^{2+}, Fe^{3+}) besides physicochemical properties of both the soil components and the agrochemicals [Lu et al., 2014; Yen et al., 2000]. As stated earlier interaction of the agrochemicals with HA as well as other NOM can either enhance the degradation process or can inhibit the same resulting in the retention of these chemicals in the environment. On one hand, the degradation process may produce more harmful metabolites that can pollute other terrestrial and aquatic bodies while on the other hand, the retention process may prevent the short–term access of these molecules to ground or surface water and their effects on non-target organisms [Arias-Estévez et al., 2008; Yen et al., 2000]. NOM/HA in aqueous medium on interaction with solar radiation can generate free radicals and reactive species such as singlet oxygen ($^1O_2$), hydroxyl radical ($^{\bullet}OH$), triplet excited state of HS and other reactive species that initiate the degradation of pollutants. NOM/HA present in soil also act as a photosensitizer where it can transfer the absorbed UV radiation to pollutants whose absorption spectra do not fall in the emission spectral region of the sun (for pollutant to undergo self-degradation in aqueous medium, they should absorb in the emission wavelength region of sun). On the other hand, NOM/HA present in soil or water decelerate the photo-degradation process by forming complexes of various stabilities [Weissenfels et al., 1992] or by trapping organic molecules in hydrophobic domains creating a kind of light-shielding effect [Arias-Estévez et al., 2008; Boguta and Soko, 2016; Chen et al., 2019; Das et al., 2019; Fang et al., 2015; Filipe et al., 2020; Gmurek and Olak-kucharczyk, 2015; Guo et al., 2019; Janssen et al., 2014; Ren et al., 2017; Silva et al., 2016; Sun et al., 2019; Wenk et al., 2013; Zhang et al., 2012]. HA can screen the sunlight as they exhibit tendency to absorb light in wide range of wavelengths including both UV and visible range.

4.1.3 NMR methods in focus

A comprehensive review of the literature confirms that interaction between HA and pollutants are generally non-covalent in nature and can be characterized by employing solution and solid-state NMR spectroscopy [Cardoza et al., 2004; Longstaffe and Simpson, 2011; Longstaffe et al., 2010; Mazzei and Piccolo, 2017; Simpson et al., 2018; Simpson and Simpson, 2014]. Being a non-destructive technique, NMR has gained worldwide attention in environmental research to assess (a) photo-degradation of pollutants and (b) both covalent and non-covalent interactions between NOM and pollutants (organic compounds, metal ions etc.) at the molecular level,

besides addressing the chemical nature of humic substances (HA) [Delort et al., 2003; Golding et al., 2005; Kohl et al., 2000; Longstaffe et al., 2016; Longstaffe et al., 2010; Longstaffe and Simpson, 2011; Mazzei and Piccolo, 2015; Simpson et al., 2007; Simpson et al., 2018; Simpson et al., 2004; Smernik 2005]. The organic compounds introduced in the environment directly or indirectly having NMR active nuclei other than ^{1}H such as ^{19}F, ^{31}P, ^{15}N, ^{13}C, etc. have enabled the researchers to explore multinuclear NMR experiments based on heteronuclei [Li et al., 2015; Nanny et al., 1997; Nanny and Maza, 2001; Strynar et al., 2004]. The related massive literature on the environmental applications of NMR can be found in the book edited by Myrna J. Simpson and André J. Simpson, 2014 [Simpson and Simpson, 2014]. It has been emphasized that comprehensive multiphase NMR (CMP-NMR) methods are the ultimate analytical methods to assess molecular interactions relevant in the field of environmental science.

In the current chapter, we aim to present a comprehensive investigation on binding interaction of monoaromatic carboxylic acid (CA) with HA (Part I) and photo-degradation of fluorinated agrochemicals in presence of HA (Part II) employing one dimensional (1D) ^{19}F solution-state NMR methods. In both the study, $^{19}F–^{1}H$ and $^{1}H–^{1}H$ STD experiments are used to probe the weak non-covalent interaction and mode of insertion of the organic molecules into HA superstructures. The molecular interactions are quantitatively detailed using 1D ^{19}F diffusion and relaxation measurements of the test molecules in presence of HA. In part I we have used commercially available Aldrich HA (AHA, isolated from lignite coal) and in case of part II we have extracted HA (KHA) from soil samples collected from the field of IIT Jodhpur campus situated at Karwar, western Rajasthan, India following International Humic Substance Society (IHSS) extraction method. Karwar soil exemplifies soils of arid region. Both the HA have been characterized and compared using ^{1}H NMR and UV-vis spectrophotometric methods. The complete extraction method described by IHSS that is used for the isolation of HA from Karwar field soil is given in section B1 of Annexure B. Molecular interactions of organic compounds with AHA are already characterized in previous literature [Albers et al., 2008; Albers and Hansen, 2010; Perminova et al., 1999] making it a model HA to establish the ^{19}F NMR methods used to analyze the agrochemical-HA interaction in solution-state. The same set of experiments can then be used for understanding the interactional behavior of extracted HA from natural soil samples. One must note here that a comparison of interactional strength of AHA and KHA are not appropriate as their genesis is completely different.

In part I of the present study we have used two mono-aromatic carboxylic acids (CA) *viz.,* 2, 6-diflourobenzoic acid (DFBA), and its non-fluorinated analog, *i.e.*, benzoic acid (BA) with AHA. Substituted benzoic acids have been extensively tested as agrochemicals especially as herbicides because of their growth regulating properties [Donaldson and Foy, 1965]. Also, it is known that the microbial synthesis and degradation of lignin generates a variety of benzene carboxylic acids and polyphenols in soil [Gerke, 2018]. Hence, it is important to understand the interaction of HS with these reactive molecules released in the environment by soil microbial activity. DFBA also appears as the ultimate degraded product of various agrochemicals such as hexaflumuron [Chaubey and Pal, 2018]. Figure 4.1 presents a consolidated graphical illustration of the said CAs-HA binding interaction. It must be pointed out that these interactions are characterized for the first time in the literature as per our knowledge [Chaubey et al., 2021].

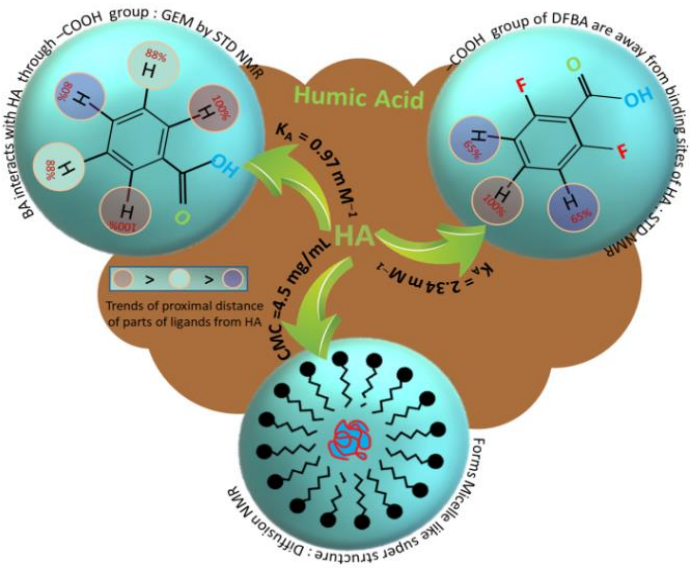

Figure 4.1: Graphical representation of the current investigation (part-I) showing binding mode and strength of investigated CAs with HA and micelle-like superstructure of AHA.

In part II, the main focus of the study is to decipher the photo-degradation behaviour of the halogen containing (fluorine and chlorine) agrochemical flupyradifurone (FPD) in the presence KHA. FPD, launched in 2014, is a representative insecticide of the novel butenolide family known as nicotinic acetylcholine receptor competitive modulators [Jeschke, 2017] exhibiting fast action on a broad range of sucking pests with an excellent field efficacy on crops [Nauen et al., 2015]. The available data on the fate of FPD in the environment suggest that it is likely to dissipate via several mechanisms of transport, *viz.*, erosion, runoff, and leaching to ground and surface water [Flupyradifurone, 2013; Glaberman and Katrina, 2014]. Also, FPD is capable of absorbing UV light and hence direct sunlight can cause natural degradation of FPD in environment. However, studies related to FPD photo-degradation and interaction with HS is limited in literature. Therefore, it is an interesting choice to investigate the effect of HA on the photo-degradation of aqueous FPD in a laboratory environment. The graphical illustration of the said investigation is given in Annexure B as figure B1 [Chaubey et al., 2020b].

4.2 EXPERIMENTAL DETAILS

4.2.1 Solution Preparations:

For NMR measurements, the stock solution of AHA, KHA, DFBA, and BA are prepared by dissolving in 0.05 M phosphate buffer (PB) of pD= 7.4±0.05 in D_2O. The stock concentrations of BA and DFBA are determined to be 10 mM for all the sets of experiments. The stock solutions of FPD and DFA of 20 mM concentration are prepared in DMSO-d_6 owing to poor solubility of FPD in aqueous solutions. For part I, 30 mg/mL stock solution of AHA and for part II, a 4 mg/mL stock solution of KHA are prepared by dissolving in deuterated PB of pD 7.4± 0.05 followed by stirring and sonication for two hours to ensure complete dissolution. Further these solutions are filtered using filter paper to remove any precipitated/ insoluble particle. The stock solutions of both AHA and KHA are found completely soluble in PB of pD 7.4± 0.05. All the other stock solutions are also sonicated before the sample preparation to ensure the homogeneous mixing of samples. For the binding experiments performed in **Part I**, a series of samples is prepared by keeping DFBA and BA concentration (1.5 mM) fixed and varying the concentration of AHA from 2 mg/mL to 25 mg/mL. For STD experiments, solutions contained 4 mg/mL AHA and 20 mM of test molecules. In case of **Part II**, all the NMR samples contained

5:95 DMSO--d_6: PB solvent ratio. The concentration of DMSO-d_6 does not exceed 5% (v/v) in total volume of the NMR solution in order to guarantee negligible influence of DMSO-d_6 on the photo-degradation rate and binding constant. For photo-degradation kinetics experiments, three samples are prepared where concentration of FPD is kept constant at 1 mM for different HA concentrations, *i.e.,* 0 mg/mL, 0.2 mg/mL and 2 mg/mL HA. These aqueous samples are exposed to the UNI-TECH UV cabinet consisting UV tube and fluorescent tube (350 W / 230 V low pressure mercury lamp) as the light source and have both short (254 nm) and long UV (365 nm) range. Mercury lamps and xenon lamps have been widely used in labs to simulate solar irradiations for photochemical environmental studies [Chen et al., 2019]. Control experiments are also performed for these samples in absence of UV irradiation for the same time duration. For relaxation and diffusion experiments, a set of seven samples is prepared by keeping FPD and DFA concentrations fixed at 1 mM and varying the HA concentrations from 0–2 mg/mL. For the STD experiments, the samples contained 0.5 mg/mL of extracted KHA and 5 mM of test molecules *viz*., FPD and DFA.

All the samples appeared clear and are equilibrated for at least an hour before recording the NMR experiments. The colour of the solutions containing HA varies from light brown to dark brown depending on the concentration of HA used. The pH of all the samples prepared is maintained at 7.4 and is measured using Orion Star A211 pHmeter equipped with a microelectrode. The viscosity of these solutions is measured using the AntonPar microviscometer with an accuracy of ±0.01 units. For UV-vis measurements, 150 μg of KHA and AHA are dissolved in 4 mL aqueous PB. It must be pointed here that the natural quantities of agrochemicals (several hundred nM to μM) and HA (few ppm or mg/L) found in the environment are in general much smaller than those used during the NMR experiments in the current study. It is necessary to choose higher concentrations (mM) of both ligand and HA to obtain better sensitivity that allows less error prone evaluation of the binding and degradation parameters of ligands in presence of HA through NMR. However, the ligand to target ratio has always been maintained similar to the ratio that is generally found in the environment. Further, the concentration used for HA is in complete agreement with the previous literature reports that detailed similar study by NMR [Mazzei and Piccolo, 2012; Šmejkalová et al., 2009; Zhao et al., 2019].

4.2.2: Details of methods

(a) UV-vis measurements:

The UV–vis absorption spectra are recorded on a VARIAN Carry 400 UV–vis spectrophotometer. The samples are scanned from 200 to 800 nm in a 10 mm quartz cuvette at temperature= 298 K.

(b) NMR measurements:

In part I, all the NMR measurements are performed at 298 K while for part II, all the NMR measurements are carried out at 295 K. ^{1}H NMR spectra with solvent pre-saturation in all the cases are obtained using Squa100.1000 shaped pulse of width 100 ms. 16 k and 8 k data points (TD) are acquired for ^{1}H NMR and ^{1}H decoupled ^{19}F NMR spectra respectively for all the systems. The specific experimental parameters related to NMR for both the parts are tabulated in table 4.1.

Table 4.1 : NMR experimental parameters used in current study. Parentheses () represent the observed nuclei for which the values of given parameters are reported.

	Part I		Part II	
Experimental parameters	**DFBA**	**BA**	**FPD**	**DFA**
SWH (ppm)	12 (^{19}F), 12 (^{1}H)	16 (^{1}H)	12 (^{19}F), 15 (^{1}H)	12 (^{19}F), 15 (^{1}H)
d1 (s)	12 (^{19}F), 15 (^{1}H)	16 (^{1}H)	2 (^{19}F), 12 (^{1}H)	12 (^{19}F), 20(^{1}H)
Relaxation measurements				
Number of scans (ns)	8 (^{19}F), 8 (^{1}H)	8 (^{1}H)	16 (^{19}F), 8 (^{1}H)	8 (^{19}F), 8 (^{1}H)
Spin echo delay (τ) (ms)	1 ms (^{19}F/^{1}H)	1ms (^{1}H)	1ms (^{19}F/^{1}H)	1ms (^{1}H)
Diffusion measurements				
ns	8 (^{19}F), 8 (^{1}H)	8 (^{1}H)	16 (^{19}F), 8 (^{1}H)	8 (^{19}F), 8 (^{1}H)
Diffusion delay (Δ) (ms)	50	50	50	20
Gradient length (δ) (ms)	1.5	1.5	3.0	1.6
STD measurements				
SWH (ppm)	50 (^{19}F), 16 (^{1}H)	16 (^{1}H)	50 (^{19}F), 16 (^{1}H)	16 (^{1}H)
ns	4096(^{19}F), 1024 (^{1}H)	1024 (^{1}H)	2048 (^{19}F), 1024 (^{1}H)	2048 (^{19}F), 1024 (^{1}H)
On-resonance frequency (ppm)	1	1	1	1
Off-resonance frequency (ppm)	40	40	40	40
Spin lock time (ms)	50	50	50	50

4.3. RESULTS AND DISCUSSION

Humic acid characterization: HAs investigated in the current study have been characterized employing UV-vis (discussed in Annexure B: section B2, figure B2 and table B1) and ^{1}H NMR methods to confirm the nature and structural complexity.

(a) ^{1}H NMR spectroscopic measurements

Kim and Yu, 2007 and Ma *et al.*, 2001 [Kim and Yu, 2007; Ma et al., 2001] have reported that ^{1}H NMR spectrum of HA is broadly divided into four regions. The first region of proton belongs to aliphatic methyl and methylene in the range (0–1.7) ppm. The second region with a range of (1.7–3.1) ppm largely contains proton attached to a carbon, generally α to the carbonyl, carboxylic, or ester group, also α to aromatic rings. The third region of ppm range (3.1–4.4) belongs to the protons of carbons attached with hydroxyl, ester, ether, and protons on methyl, methylene carbon that are directly bonded to O and N. The forth region (6–8.5) ppm consist of aromatic protons of phenols and quinones. However, the number of peaks in these four different regions generally varies depending upon the soil type, location, and extraction technique. Figure 4.2 represents solvent suppressed ^{1}H NMR spectrum of commercially purchased Aldrich HA (AHA), while (b) shows a similar spectrum for extracted HA (KHA) from the soil of IIT Jodhpur Karwar.

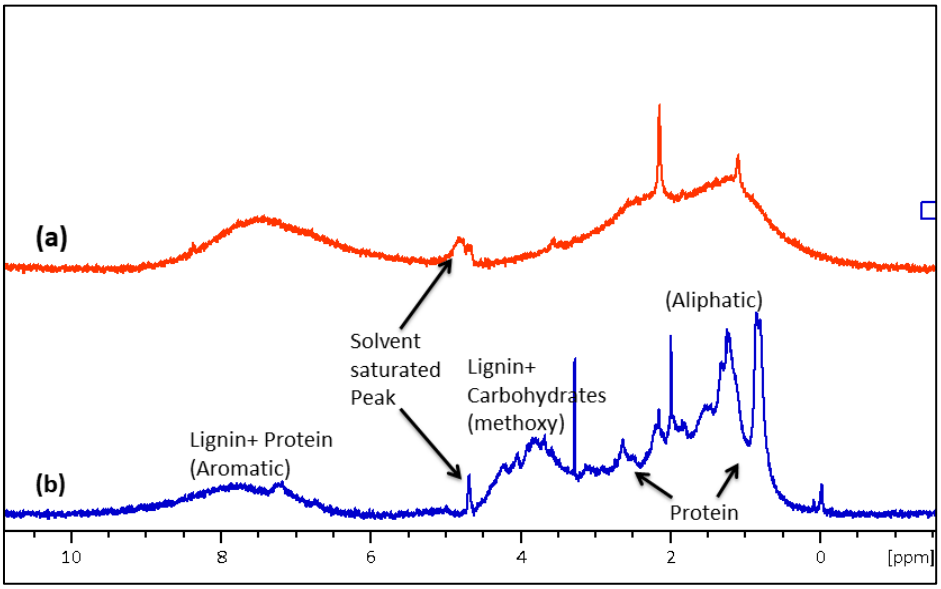

Figure 4.2: Solvent Residual proton (HOD) peak suppressed ^{1}H NMR spectra of (a) AHA) (b) KHA at pH=7.4 and T=298 K

The relative soil components have been assigned in the spectrum following the literature [Albers and Hansen, 2010; Longstaffe et al., 2010; Saito and Hayano, 1981; Simpson et al., 2004]. Several peaks appeared in the aliphatic region (0–5 ppm region), and a broad hump is seen in the aromatic region (6–10 ppm) for both HAs. These spectra matched very well with the literature reported HA spectra; including the characteristic aromatic HA peak at 8.4 ppm. Kang et al., 2002 has explained that the presence of broad hump like peaks in NMR spectra represents the amount of humification [Kang et al., 2002]. Further, it must be mentioned here that the appearance of very broad peaks in ^{1}H NMR spectra of HA is representative of fast relaxation rates characteristic of macromolecular structures leading to the broadening of a signal. This observation indicates possible aggregation and/or association of humic molecules. It has already been discussed in the literature that humic molecules tend to aggregate either to form micelle like structure or superstructures due to their characteristic chemical composition giving rise to such broad peaks in NMR [Mazzei and Piccolo, 2012]. From the NMR spectrum shown in figure 4.2, a clear difference in the structure of AHA and KHA can be pointed out: KHA possesses clear, sharp peaks in the aliphatic region compared to AHA. Approximate aromatic and aliphatic contents have been determined for both the HA by integrating the peaks in 6–10 ppm and 1–4.5 ppm region, respectively. KHA has been found to bear 12.5% aromatic and 87.5% aliphatic residues in comparison to AHA possessing *ca.* 26% aromatic and 74% aliphatic residues. This matches with the analysis made by UV-Vis measurements given in Annexure B: section B2. Figure 4.2 also depicts that the average structure of both HAs shown significant similarities as well as differences that could influence their interaction with organic pollutants. Also, to confirm the effect of 5% DMSO-d_6 on the KHA structure, both NMR and UV data of KHA prepared in 5: 95 DMSO: aqueous PB (pH=7.40) are also recorded. Both the spectra matched exactly with NMR and UV spectra of KHA recorded in aqueous PB (pH=7.40) solvent confirming insignificant effect brought by the 5: 95 DMSO: aqueous PB solvent on the structure of KHA.

Further, to probe the micelle like nature of both HAs, ^{1}H NMR self-diffusion coefficient (D) measurements are recorded for AHA and KHA protons with increasing HA concentration employing BPPLED diffusion pulse sequence. Diffusion NMR spectroscopy is one of the powerful tools to probe aggregation of the molecules by determining the D values. It is well known from the studies conducted on surfactants that translational diffusion also shows

marked change when the molecule undergoes aggregation or micelle formation above a threshold concentration known as critical micellar concentration (CMC) similar to various other physical parameters [Šmejkalová and Piccolo, 2008a]. The CMC for AHA is determined, as shown in figure 4.3, following the literature report [Šmejkalová and Piccolo, 2008a]. On the other hand, *D* values for EHA showed continuous decrease and any such sharp breakpoint does not appear for EHA. It suggests that KHA do not form pseudomicelles in the investigated concentration range.

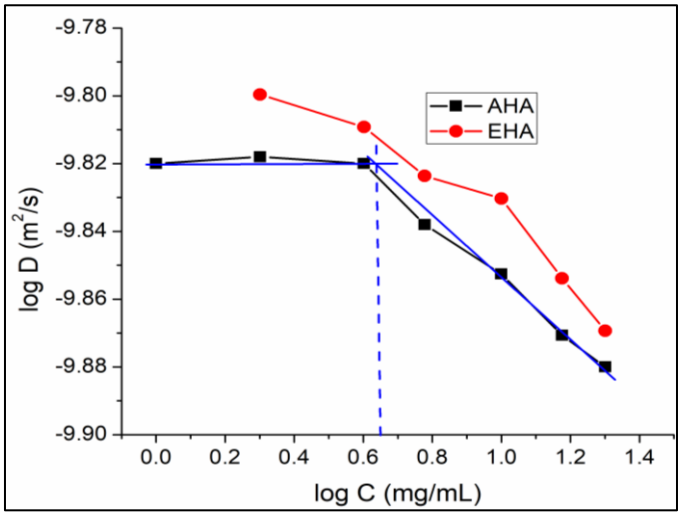

Figure 4.3: Influence of increasing concentration of AHA and KHA on diffusion coefficients (*D*) of AHA and KHA aliphatic protons at pH=7.40 and *T*= 298 K.

Figure 4.3 demonstrates a significant decrease in average *D* values after 4 mg/mL with increasing HA concentration. The decrease in average *D* values accounts for decreased mobility resulted due to aggregation or superstructure formation of HA molecules. From the breakpoint, the CMC for AHA is determined to be 4.5 mg/mL. The diffusion measurements provided evidence of the micellar nature of HA possessing hydrophobic as well as hydrophilic domains imparting the potential to encapsulate organic pollutants in these micellar domains. A rough estimate of the molecular weight of AHA from the *D* values can be determined by comparing it with known standards, reported by Piccolo and co-workers [Šmejkalová and Piccolo, 2008a]. In the current study, the nominal molecular weight of AHA is assumed to be in the range of 3,000 Da – 7,000 Da (as found from their *D* values) and used for further calculations. This assumption matched well with the previous report by Chin and co-workers, 1997, for Aldrich HA, having a molecular weight of 4,100 [Chin et al., 1997]. It has to be mentioned that the present study aims to use the approximate value of the molecular weight to compare the relative binding strength of AHA–DFBA and AHA–BA system under investigation discussed in the next section rather than determining the exact molecular weight of AHA.

4.3.1: Part I: Monoaromatic carboxylic acids with humic acid

(i) Characterization of the interaction between AHA–DFBA and AHA–BA by NMR:

The section presents a qualitative and quantitative evaluation of HA–CA interaction by employing relaxation and diffusion measurements. A detailed analysis of chemical shift changes is also reported.

(a) ^{19}F and ^{1}H NMR linewidth (FWHM) and chemical shift:

Both ^{1}H and ^{19}F 1D NMR spectra have been recorded for the test molecules in the presence and absence of HA. In the case of DFBA, ^{19}F NMR has proven to be more sensitive compared to ^{1}H NMR owing to the wide chemical shift range for ^{19}F yielding chemical shifts and peak widths sensitive to the changes in the local as well as macroscopic environments [Dixon et al., 1999]. ^{1}H NMR spectra of DFBA and BA with and without HA along with their respective molecular structures are shown in figure 4.4. The effect of concentration of AHA on ^{1}H coupled ^{19}F NMR, and ^{1}H decoupled ^{19}F NMR spectra of DFBA have been shown in Annexure B as figure B3. Both DFBA and BA exhibit non-first order ^{1}H spectra indicating the existence of strong ^{1}H–^{19}F and ^{1}H–^{1}H through bond coupling. The ^{1}H NMR spectrum of the free DFBA consists of two ^{1}H peaks, one at 6.93 ppm (coupled with F and H_a) and second at 7.29 ppm (coupled with H_b and F) owing to the presence of two chemically inequivalent protons as shown in the structure of DFBA. On the other hand, three NMR peaks appeared for BA at 7.40 ppm (coupled with H_b and H_a), 7.47 ppm (coupled with H_c and H_b), and 7.81 ppm (coupled with H_c and H_a) corresponding to three chemically inequivalent protons H_c, H_a, and H_b respectively. In the case of the ^{19}F NMR spectrum of DFBA, due to the presence of equivalent fluorine, the appearance of a single ^{19}F peak is noted (figure B3 (b), bottom trace: Annexure B).

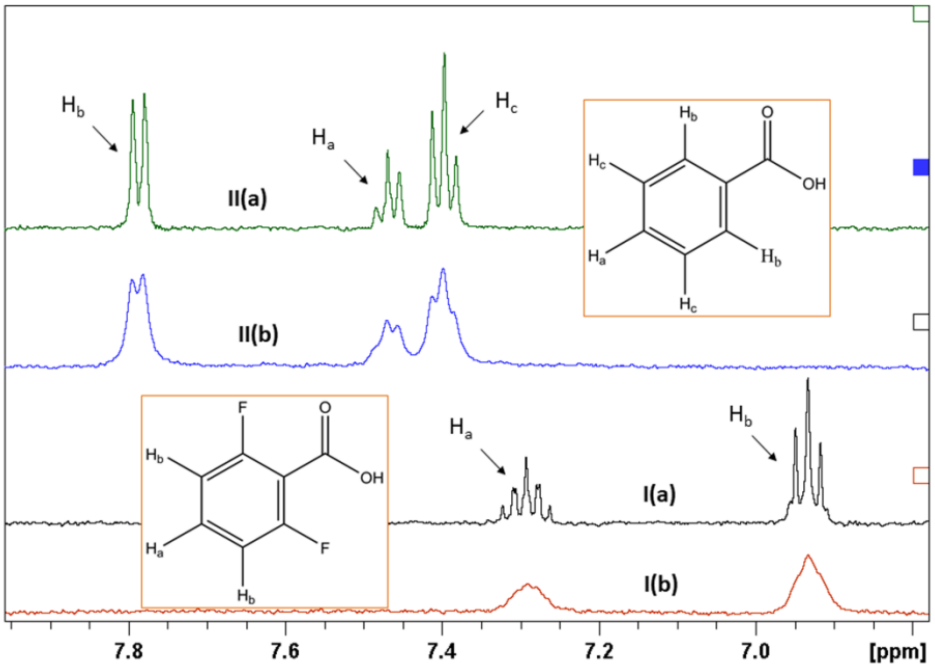

Figure 4.4: ^{1}H NMR spectrum of (I) DFBA (II) BA in (a) absence of AHA and in (b) presence of 5 mg/mL AHA at pH=7.4 and T=298 K

Further, on the addition of 5 mg/mL of AHA to the solution of DFBA and BA, ^{1}H and ^{19}F (in case of DFBA only) NMR peaks are broadened significantly. Also, the appearance of a single ^{1}H and ^{19}F peaks indicates a possible association of the test molecules with HA falling in the fast chemical exchange regime [Bain, 2003; Chaubey and Pal, 2018]. The ^{19}F and ^{1}H line broadening noted for both the systems increases progressively with increasing concentration of AHA, as shown in Annexure B as figure B3 and B4. For example, the ^{19}F peak FWHM changed from 2.37 Hz to 9.19 Hz on the addition of 5 mg/mL AHA. However, no significant change in the ^{1}H chemical shift for both DFBA and BA is observed with the addition of AHA, while ^{19}F NMR of DFBA showed infinitesimal drift in the ^{19}F chemical shift (~0.01 ppm) for DFBA with the

addition of AHA. These observations are in agreement with literature [Nanny and Maza, 2001; Simpson et al., 2004].

(b) Saturation transfer difference experiments:
To confirm the preliminary observation of binding obtained from chemical shift and line-broadening measurements, a set of $^{19}F–^{1}H$ and $^{1}H–^{1}H$ STD NMR experiments are carried out. The STD spectrum of AHA has also been subtracted in STD_{diff} spectrum. The same experiment has also been repeated by selectively saturating the aromatic protons of AHA near 8.0 ppm and similar trends are seen for BA and DFBA as obtained by saturating aliphatic protons. Hence, it can be said that the average orientations of the CAs do not change in different domains of AHA regardless of the fact from which part of AHA the saturation originates. Figure 4.5 (I and II) shows the $^{1}H–^{1}H$ STD spectra for DFBA–AHA and BA–AHA system, while figure 4.5 (III) shows the $^{1}H–^{19}F$ STD spectrum for DFBA–AHA system. The saturation transferred to each proton is calculated by integrating the proton peak that appeared in STD_{diff} relative to STD_{off} employing equation 2.22 as discussed in chapter 2 (section 2.6) [Mayer and Meyer, 1999]. A close inspection revealed that saturation transferred to proton near to the carboxylic acid group is greater than that of other protons in the case of BA, while a reverse case is seen for DFBA. In the case of BA–AHA protons, maximum saturation is received by proton H_b (100%) compared to the other two protons (H_c: 88% & H_a : 80%) indicating BA binding to AHA through the carboxylic acid group of BA. While, in the case of DFBA–AHA, H_a (100%) experienced the highest saturation transfer compared to H_b (65%), confirming non-fluorinated functional groups are oriented away from the AHA during the interaction. Hence, the presence of a fluorinated group induces a differential binding mode in the aromatic compound. A peak of significant intensity appeared in $^{1}H–^{19}F$ STD difference spectrum that further confirms the interaction between DFBA and AHA.

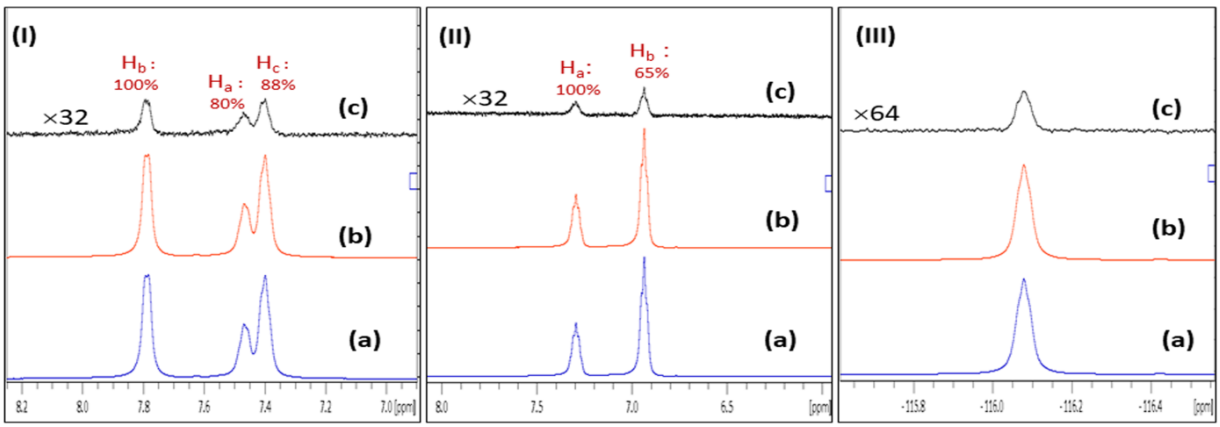

Figure 4.5: NMR (a) STD_{off} (b) STD_{on} and (c) STD_{diff} spectrum for systems (I) BA–AHA ($^{1}H–^{1}H$) (II) DFBA–AHA ($^{1}H–^{1}H$) (III) DFBA–AHA ($^{1}H–^{19}F$) at pH=7.40 and T=298 K. [AHA]=4 mg/mL; [BA]=20 mM; [DFBA]=20 mM

(c) Relaxation measurements: A comparison of the T_1 and T_2 values for DFBA/BA in the absence and presence of AHA can provide valuable information about the strength of the binding with AHA. Figure 4.6 (a and b) displays the representative plot of ^{1}H and ^{19}F relaxation times T_1 and T_2 respectively measured for DFBA and BA as a function of AHA concentration. The corresponding T_1 and T_2 values are given in Annexure B as table B2 and table B3. From the figure 4.6, it can be seen that (a) both the relaxation times (T_1 and T_2) decrease monotonically with increasing AHA concentration for both DFBA and BA; (b) the change in ^{19}F T_2 of DFBA is of a greater extent than ^{19}F T_1 of DFBA since ^{19}F T_2 is more sensitive towards molecular

interaction compared to ^{19}F T_1 as per literature [Dalvit, 2007; Gerig, 1997]. Such behavior of ^{19}F relaxation could be attributed to the effect of CSA as a pronounced relaxation mechanism in solution at the high magnetic field [Gerig, 1997]; (c) the changes in ^{19}F T_2 for DFBA are found larger compared to ^{1}H T_2 for DFBA that can be interpreted to have arisen due to hydrogen bond formation between ^{19}F nucleus and AHA [Dixon et al., 1999]. Such hydrogen bonding is known to have pronounced effect on ^{19}F relaxation times; (d) Moreover, the major changes in T_1 and the T_2 value are observed for lower (initial) concentrations of AHA suggesting that majority of DFBA/BA bind to AHA during initial additions of AHA; (e) Also, the percentage decrease in T_1 and T_2 values for DFBA is of greater extent than BA in the presence of the same concentration of HA. For example, the change in $^{1}H_a$ T_1 for DFBA in the presence of 5 mg/mL HA compared to free DFBA is 65%, while for a similar concentration of BA (H_b), it is 49% only. It demonstrates that fluorinated molecule (DFBA) participates in more rigid binding to AHA than its non-fluorinated analogue (BA). An additional point to be noted here is that the values of ^{1}H relaxation times for different protons of DFBA (H_a, H_b) and BA (H_a, H_b, H_c) are different in the absence of HA. On the other hand, the progressive addition of HA results in very similar T_1 values for various protons of DFBA/BA. Thus global molecular motions become prominent over local motions with the addition of HA [Nanny and Maza, 2001; Šmejkalová and Piccolo, 2008b; Šmejkalová et al., 2009]. This observation, in conjunction with a lack of significant change in their chemical shift, confirms the presence of strictly non-covalent interaction between the test molecules and HA.

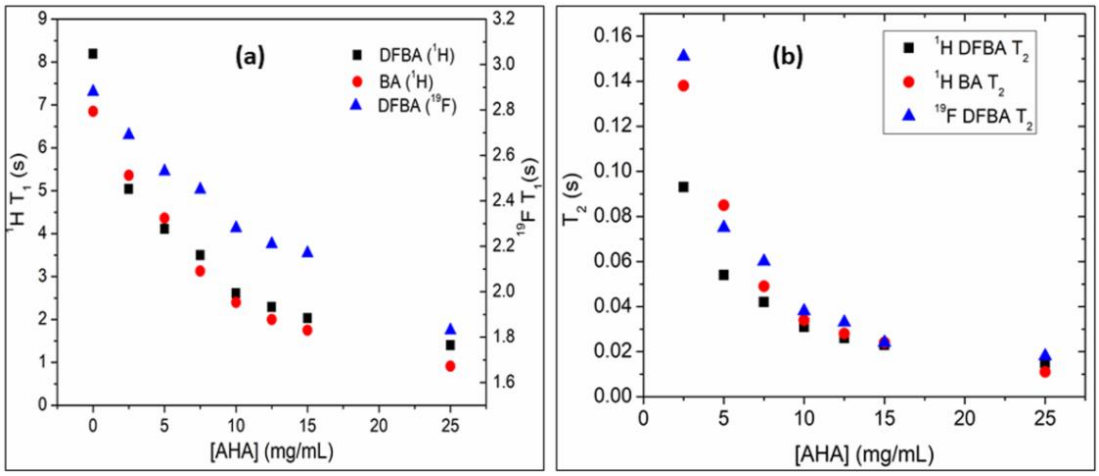

Figure 4.6: Graphical representation of measured ^{19}F and ^{1}H NMR (a) T_1 and (b) T_2 for DFBA and BA as a function of AHA concentrations (mg/mL) at 298 K and pH 7.4.

Further, molecular correlation time (τ_c) has been extracted for the test molecules in the presence of HA and plotted as a function of HA concentration in figure 4.7. In the present case, τ_c is calculated following works of W. R. Carper and C. E. Keller, 1997, and W.R. Carper* and E. A. Nantsis,1998 [Carper, 1999; Carper et al., 2002] using equation 4.1 for viscous systems (CA in the presence of HA).

$$\tau_c(ns) = a_0 + a_1(R_2/R_1) + a_2(R_2/R_1)^2 + a_3(R_2/R_1)^3 + a_4(R_2/R_1)^4 \text{.....(4.1)}$$

a_0, a_1, a_2, and a_4 are constant coefficients that depend on the magnitude of the magnetic field used and the nucleus observed.

For free DFBA and BA, τ_c is determined from the measurements of ^{13}C T_1 that is considered to be purely dipolar in nature. A closer inspection of figure 4.7 (data are given in table B2 and B3: Annexure B) revealed that correlation times increased with increasing HA

concentration, indicating an entrapment of these aromatic CA within humic domains. With the addition of HA, τ_c of free test molecules increases *ca.* by two orders of magnitude *i.e.,* from 10^{-11} to 10^{-9} for both DFBA and BA. The increase in correlation time is most prominent for the DFBA–AHA system than for the BA–AHA system, *i.e.,* 195 times increase for DFBA in 2.5 mg/mL HA compared to free DFBA and 175 fold increase for BA in 2.5 mg/mL HA compared to free BA. Further, a 20% increase in τ_c calculated by monitoring H_a is observed for DFBA–AHA from 2.5 mg/mL AHA to 5 mg/mL AHA compared to only 11% increase in τ_c for BA–AHA for the same concentration. This observation also supported the finding that fluorinated molecule DFBA is a better binder to HA than BA.

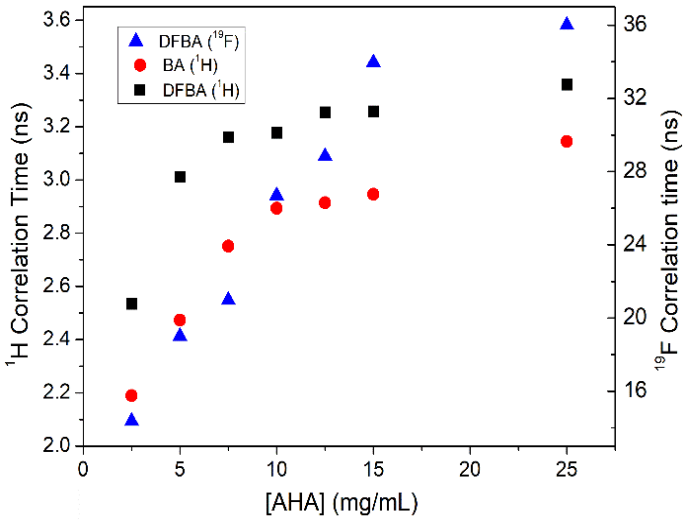

Figure 4.7: Graphical representation of correlation times (τ_c) extracted for DFBA and BA from ^{19}F and ^{1}H T_1 and T_2 values as a function of AHA concentrations (mg/mL) at 298 K and pH 7.4

In the following section, NMR diffusion measurements have been carried out to quantify the binding interaction of test CA molecules with AHA.

(d) Diffusion measurements:

According to Stoke-Einstein's description, a small molecule experiences a decrease in D value due to an increase in hydrodynamic radius as a consequence of binding to a macromolecule leading to an increase in its molecular size [Johnson, 1999]. Therefore, the measurement of small molecule D value in the presence of HA would reflect their binding to HA. In the present case, hydrodynamic radius (r_H) of DFBA and BA are determined from their measured D values in the free and bound form using the Stokes-Einstein relation (equation 2.19, chapter 2, section 2.5) and is found increasing as a function of AHA concentration. It clearly accounts for the association of DFBA/BA within AHA that led to an increase in r_H of BA and DFBA. For a fast exchanging system on the diffusion time scale (~100 ms), the observed diffusion coefficient of a small molecule in the presence of the macromolecule is a weighted average value of the diffusion coefficient in its free and bound state as expressed in equation 2.21, chapter 2 (section 2.5) [Wimmer et al., 2002]. In line with the literature, $D_{complex}$ for the DFBA−AHA/BA−AHA complex has been approximated to the free AHA diffusion coefficient; the small molecules on complete binding would acquire the properties of HA [Mazzei and Piccolo, 2012]. Hence, ^{1}H D values for protons of AHA is determined for different concentrations of AHA to obtain value of D_{complex}. Further, the D values measured for DFBA/BA in the presence of HA denoted as ($D_{DFBA,\ obs}$) are used to determine the bound fraction of DFBA (P_b) as per equation 2.21. NMR observables such

as T_1, T_2 can also be used to quantify P_b using equation 2.21. However, P_b is, in general, heavily overestimated by such relaxation measurements [Mazzei and Piccolo, 2015]. It can be explained by the fact that T_1 values are more sensitive towards the local modification of the chemical environment, while diffusion values are affected by global changes only. Such changes could be due to alteration of solution viscosity too. As per Stoke-Einstein's relation, increased viscosity of the solution also decreases the diffusion due to restricted mobility. Hence, the effect of solution viscosity must be taken into account while quantifying the association of small molecules with macromolecules employing diffusion measurements [Wimmer et al., 2002]. Therefore, in the present case, the measured diffusion coefficients for DFBA and BA are viscosity corrected as per the following equation 4.2:

$$D_{DFBA}[HA] = D_{DFBA,app}[HA] \times \frac{\eta[0]}{\eta[sol]} \text{.....(4.2)}$$

where, η: dynamic viscosity (Pa-s); $[HA]$:concentration of Humic acid (mg/mL) ; $D_{DFBA,app}[HA]$: measured diffusion constant of DFBA at HA concentration ; $D_{DFBA}[HA]$: viscosity corrected diffusion constant.

The raw and viscosity-corrected ^{19}F and ^{1}H diffusion coefficients (D) for DFBA and BA as a function of AHA concentration are presented in figure 4.8 and table B4: Annexure B2.

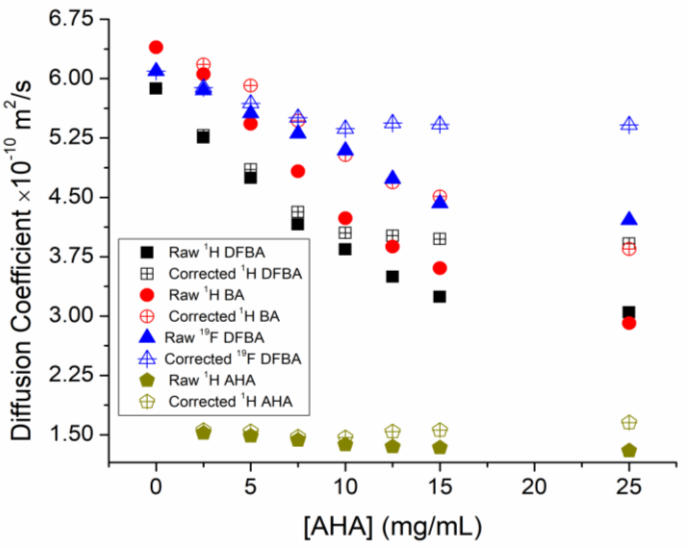

Figure 4.8: Average observed (raw) *D* values and viscosity corrected ^{19}F & ^{1}H *D* values for DFBA, BA and AHA signals as function of increasing concentration of AHA (mg mL^{-1}) at 298 K and pH 7.4.

The D values of the test molecules are always found to be decreasing with increasing concentration of AHA compared to the free test molecules in both cases. The change in D values for DFBA in the presence of AHA with respect to the free DFBA is found to be of greater extent than that of BA in the absence and presence of AHA. Nearly 31% decrement in D value is observed for DFBA on the addition of 10 mg/mL AHA while only a 21% change in D value is noted for similar BA concentration. For the DFBA-AHA system, the observed D values reached a plateau after 10 mg/mL AHA concentration, while for the BA–AHA systemthe D values exhibited a monotonic decrease. These results are concurrent with the calculated bound fraction for DFBA as a function of AHA concentration shown in figure 4.9 (a) where the constant value of P_b appears from 10 mg/mL-20 mg/mL AHA. It represents that after a threshold concentration of 10 mg/mL, DFBA binding to AHA attains saturation. On the other hand,

BA–AHA represents a weaker interaction compared to DFBA–AHA, where P_b value shows a progressive increase as a function of AHA concentrations [Šmejkalová et al., 2009]. Figure 4.9 (b) demonstrates a representative plot of extracted P_b from ^{1}H D_{DFBA} values as a function of AHA concentration. Similar plots for BA and DBFA using ^{1}H D_{BA} and ^{19}F D_{DFBA} values are given as figure B5 (a & b) (Annexure B). These plots of P_b calculated for DFBA/BA against the concentration of free AHA (figure 4.9 (b) and figure B5) is fitted with (a) Langmuir adsorption model, where all the binding sites are assumed to be identical and with (b) modified Langmuir adsorption model (given in equation 4.3, and 4.4) considering wide chemical heterogeneity of humic superstructures. HS can have different types of domains exposed for interaction with guest through weak dispersive forces [Koopal et al., 2005; Mazzei and Piccolo, 2012].

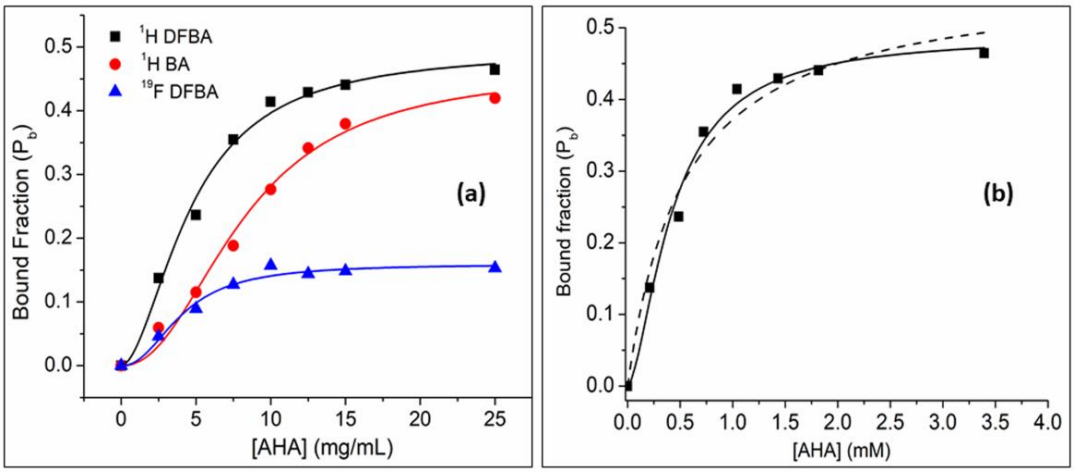

Figure 4.9: Bound fraction calculated for bound DFBA and BA from their ^{1}H and ^{19}F *D* values as a function of AHA concentration (b) Representative plot showing K_A determination for DFBA using P_b values calculated from ^{1}H D_{DFBA} values. (In figure 4.9 (b), solid line and the dashed line represent the fitting obtained by Modified Langmuir model and Langmuir model respectively).

Equation 4.3 and 4.4 written below for HA widely known as Langmuir equation and modified equation (Langmuir-Freundlich-Hill) have been used to determine K_A.

$$P_b = \frac{\alpha.K_A.[HA]}{1+K_A.[HA]} \text{.....(4.3)} \qquad P_b = \frac{\alpha.(K_A.[HA])^n}{1+(K_A.[HA])^n} \text{.....(4.4)}$$

Here, α is an offset constant added for proper fitting. While writing equation 4.3, all binding sites were assumed to be identical and the global fits are performed for $n = 1$. In equation 4.4 $n \neq 1$ accounts for multiple bindings or heterogeneity in binding, K_A is an average association constant for binding of test molecules on various HA sites, [HA] represents concentration of free or unbound HA. In this case, in order to account for complexes of different stoichiometry, the value of n in equation 4.4 needs to be adjusted to higher powers. In our calculations, the heterogeneity of humic materials is taken into account and n is left "unlocked" during fitting procedures. An improved fitting of the experimental points is achieved with the modified Langmuir model (n ≠ 1) compared to that of the Langmuir equation (n=1), as evident from the respective R^2 values. The fitting process enabled the determination of the association constant (K_A) that is further used to compare the complex stability of DFBA and BA with HA. The extracted bound fraction P_b is used here to quantify free HA concentration using the following relation given in equation 4.5.

$$[HA] = [HA]_0 - P_b[DFBA]_0 \text{.....(4.5)}$$

Moreover, K_A determined from the aforesaid fitting allowed the calculation of Gibbs free energy of transfer ($\Delta G°$) for DFBA/BA interaction with AHA given as [$\Delta G° = -RT \ln K_A$] [Mazzei and Piccolo, 2012]. Values of K_A and $\Delta G°$ are reported in table 4.2.

Table 4.2: Calculated binding constant (K_A) and Gibbs free energy of transfer ($\Delta G°$) for the association of CAs with AHA at 298 K and pH=7.4.

Sample	K_A (mM^{-1}) (Modified Langmuir model)	R^2	K_A (mM^{-1}) (Langmuir model)	R^2	ln K_A	$\Delta G°$ (kJ/mol)	K_A (mL mg^{-1})
DFBA–AHA	2.345±0.242	0.986	1.868±1.097	0.961	7.760	−19.226	0.217±0.017
BA–AHA	0.971±0.077	0.985	0.385±0.916	0.940	6.878	−17.040	0.117±0.010

*Source of errors is average standard deviations calculated from independent experiment

K_A values are determined in both the units of mL/mg and mM^{-1} with the former unit representing more reliable K_A values. A negative value of $\Delta G°$ reported for both the systems at pH 7.4 indicated the binding of DFBA and BA to HA as a thermodynamically favorable and spontaneous interaction process. The reported K_A in mM^{-1} range denotes moderate to weak binding between test molecules and AHA. On comparing the values of K_A for both the systems, it has appeared that the association of DFBA to AHA is nearly 2.4 times greater than that of BA–AHA complex. The substitution of fluorine atoms on the aromatic ring invokes differential binding strength of the fluorinated CA in addition to the differential binding mode. BA prefers to bind to AHA through the carboxylic acid group, probably by –H bonding. On the other hand, –F substituted DFBA undergoes interaction with AHA keeping non-fluorine functional group oriented away from AHA. It is well known that –F being electronegative atom can pull electron density away from the C atoms creating a dipole with a partial negative charge on –F and a partial positive charge on –C. Such a dipole generation will allow –F to interact with polar species through potential hydrogen bonding and dipole-dipole interaction. In the carboxyl group, the oxygen atom is more electronegative than the attached C atom; thus the C=O is treated as polar dipole and may interact similarly as the C–F groups. However, the apparently stronger dipole generation by more electronegative F at pH 7.4 than –COOH would result in stronger molecular interaction in solution compared to a non-fluorinated molecule containing only CA [Shirzadi et al., 2008b].

(ii) DFBA interaction with KHA and its comparison with AHA.

The binding of DFBA with KHA has been quantified and compared with that of AHA. It is well established in the literature that the structures (size and charge) of humic and fulvic acids are dynamic with regard to environmental conditions [Klučáková, 2018]. As discussed in the previous section, the present AHA exhibits higher molecular mass, humification degree, and presence of condensed aromatic structures compared to KHA as evident from its UV E_4/E_6 and E_2/E_6 values and ^1H NMR analysis. These differences in the structural and chemical properties of KHA can influence the extent of the binding of organic molecules. Figure 4.10 compared the ^1H and ^{19}F NMR spectrum of DFBA in the absence and presence of AHA and KHA. Further, relaxation rates and diffusion coefficient of DFBA have been measured in the presence and absence of KHA to compare the extent of binding. Table 4.3 reports the changes in the values of these relevant NMR parameters, namely linewidth, T_1, T_2, and D values for DFBA due to the addition of AHA and KHA.

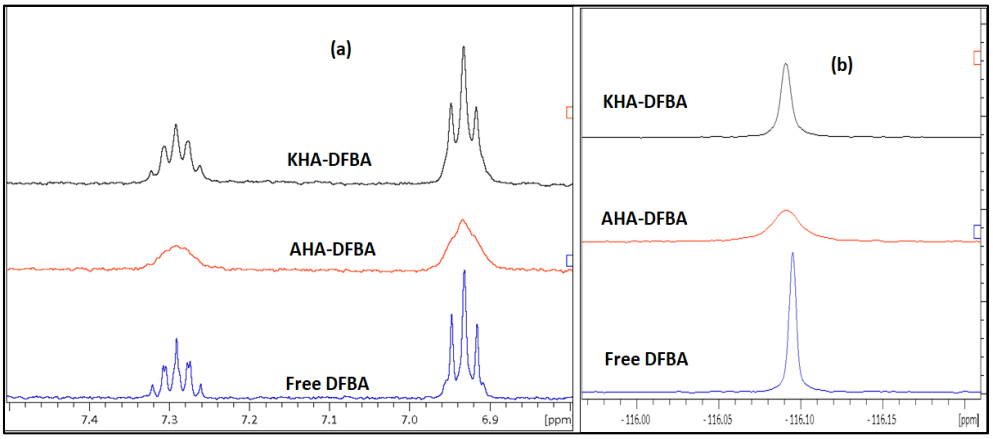

Figure 4.10: (a) ^{1}H NMR (b) ^{19}F NMR spectra of 2 mM DFBA in presence and absence of 5 mg/mL AHA and KHA.

Table 4.3: Relevant NMR parameters, *i.e.*, line width at full width-half maximum (FWHM), relaxation time (T_1 & T_2) and diffusion coefficient for DFBA (2 mM) in the absence and presence of 5 mg/mL AHA and KHA

Sample	FWHM (Hz)			T_1 (s)			T_2 (s)			Average D $\times 10^{-10}$ m^2/s	
	^{19}F	^{1}H$_a$	^{1}H$_b$	^{19}F	^{1}H$_a$	^{1}H$_b$	^{19}F	^{1}H$_a$	^{1}H$_b$	^{19}F	^{1}H
Free DFBA	2.37	15.40	14.80	2.85	8.19	7.16	2.28	5.78	5.15	6.09	6.40
AHA+DFBA	9.20	19.82	21.90	2.52	2.90	2.41	0.08	0.05	0.04	5.80	5.91
KHA+DFBA	3.59	15.99	15.31	2.73	4.79	3.90	1.05	0.81	0.85	5.91	6.24

A close inspection of the spectrum shown in figure 4.10 and table 4.3 reveals that the changes in NMR parameters for DFBA with the addition of HA are of larger extent in the case of AHA–DFBA than KHA–DFBA. ^{19}F T_1 measured for DFBA showed a change of 11% in the case of DFBA–AHA and 5% only in the case of KHA, while percentage change in ^{19}F T_2 is 96 % (DFBA–AHA) and 54% (DFBA–KHA) respectively. Similarly, a percentage change of ~65% in ^{1}H T_1 and ~99% in ^{1}H T_2 is observed for DFBA in the presence of AHA while on the other hand in the presence of KHA, these changes are only 41% in case of T_1 and 83% in case of T_2 relaxation. Similar changes can be seen in their τ_c and diffusion values. This set of preliminary data indicates that the extent of binding of DFBA to HA be greater for AHA compared to KHA. Therefore, it can be concluded that AHA is a stronger binder to DFBA compared to the present KHA in similar solution conditions. For explicit quantification of the association constants, all previous set of diffusion measurements should be performed for AHA–DFBA/BA system.

4.3.2: Part-II: Halogenated agrochemicals with humic acid

This section narrates the findings of the present study by documenting the solution-state NMR measurements and subsequent analysis to decipher a) photo-degradation of FPD, b) the effect of KHA on the photo-degradation kinetics and c) quantification of the molecular interaction between FPD and KHA in the aqueous medium.

(i) Molecular behaviour of FPD in presence of HA: NMR evaluation

(a) NMR spectra of FPD in absence and presence of HA: Figure 4.11 (I) and (II) respectively represent the ^{1}H and ^{19}F NMR spectra of FPD in absence and presence of KHA along with the FPD molecular structure with proton numbering. The complete spectral analysis is provided in table 4.4.

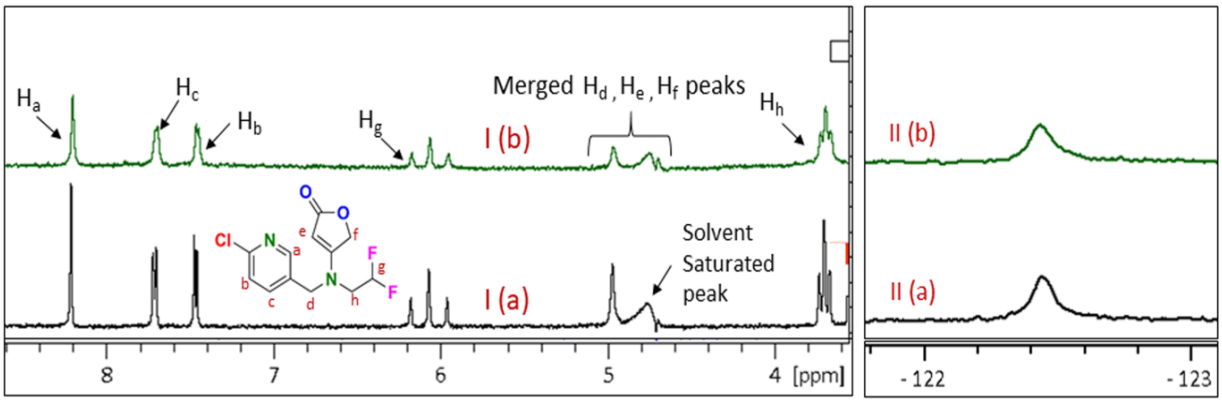

Figure 4.11: (I) Solvent presaturated ^{1}H NMR and (II) ^{19}F NMR of FPD in (a) absence and (b) the presence of 1 mg/mL of KHA prepared in 5: 95 DMSO: aqueous PB solvent system and recorded at 295 K. (pH=7.40)

Table 4.4: ^{1}H and ^{19}F NMR spectral analysis in terms of chemical shift and coupling patterns for FPD and DFA prepared in 5: 95 DMSO: aqueous PB solvent system (pH=7.40), T=295 K.

Molecule	Nuclei	Coupling partner	Multiplicity	Magnitude of coupling strength (J_{xy}) (Hz)	Chemical shift (ppm)
FPD	H_a	H_c (long range)	Doublet	J_{ac} = 1.78	8.38
	H_b	H_c	Doublet	J_{bc} = 8.37	7.48
	H_c	H_b and H_a (long range)	Doublet of doublet	J_{cb} = 8.36 J_{ca} = 1.80	7.79
	H_d	H_a (long range) & H_c (long range)*	Doublet of doublet*	……	4.91 (merged with solvent, H_e and H_f peak)
	H_e	----------	Singlet*	……	4.91 (merged with solvent, H_d and H_f peak)
	H_f	----------	Singlet*	……	4.91 (merged with solvent, H_e and H_d peak)
	H_g	H_h and F	Triplet of triplet	J_{gh} = 2.90 J_{gF} = 54.25	6.29
	H_h	H_g and F	Triplet of doublet	J_{hF} = 15.30 J_{hg} = 2.80	3.75
	F	Nearby F, H_g and H_h	Unresolved multiplet due to strong coupling		–122.48
DFA	H_a	F	Triplet	J_{aF} = 54.97	5.76
	F	H_a	Doublet	J_{Fa} = 54.91	–124.08

***** represents expected peak coupling pattern and multiplicity for the peaks that are unresolved or are not seen in the NMR spectrum

With the addition of KHA, both ^{1}H and ^{19}F NMR peaks for FPD have undergone line-broadening with minor drift in their chemical shift values. Similar ^{1}H and ^{19}F spectra of FPD are presented in figure B6 (Annexure B) recorded as a function of increasing KHA concentration. NMR peak linewidth has increased progressively with increasing KHA concentration while the change in chemical shift is modest both in case of ^{1}H and ^{19}F indicating possible non-covalent

interactions between FPD and KHA [Nanny and Maza, 2001; Simpson et al., 2004]. A preliminary analysis of ^{1}H spectral line-broadening as a function of KHA concentration reveals that the most prominent changes have occurred for protons present in the pyridine (aromatic) ring with –Cl substituent representing interaction with KHA preferably through the aromatic pyridine moiety. One must note here that a single set of peaks appear for FPD in presence of KHA that indicates molecular association between FPD and KHA falling in the fast exchange regime on NMR chemical shift time scale [Bain, 2003]. The molecular interaction of FPD with KHA may play a significant role in altering the degradation rate or degradation mechanism. It is, therefore, of interest to analyse the effect of aqueous KHA on the photo-degradation behaviour of FPD.

(b) Aqueous photo-degradation of FPD in the absence and presence of KHA

Degradation of agrochemicals due to hydrolysis or photolysis in aqueous media can be heavily influenced by organic matters as per literature reports [Chen et al., 2019; Chiron et al., 1995]. Accordingly, the fate of aqueous FPD sample in presence and absence of dissolved KHA is analysed by monitoring the changes in ^{1}H and ^{19}F NMR spectra of FPD as a function of time to answer whether FPD is (a) likely to undergo hydrolysis on its own, (b) prone to aqueous photolysis in the presence of UV radiation and (c) the effect of KHA on such degradation processes of FPD.

***Case (a)*:** The spectral changes in the ^{1}H and ^{19}F NMR of FPD in aqueous PB (pH = 7.4) in the absence and presence of KHA and without exposure to sunlight or UV radiation are monitored at a regular interval of three hours. In both cases, no significant changes in terms of appearance and disappearance of new ^{1}H and ^{19}F NMR resonances for FPD are observed with time (up to 100 hours). These observations indicate that FPD is not prone to hydrolysis on its own, and dissolved KHA has no significant role to play in modifying the hydrolytic degradation behaviour of FPD.

***Case (b)*:** In order to unravel the behaviour of FPD under photolytic condition, aqueous FPD solution is further exposed to natural sunlight as well as UV light in UV-Cabinet considering the fact that in real natural conditions sunlight will be the ultimate source of UV radiation for these agrochemicals to undergo aqueous photolysis. It has already been demonstrated in previous studies that different UV light sources *viz*., various UV lamps and natural sunlight generate identical degradation products in similar solution conditions with different degradation kinetics [Sevilla-Morán et al., 2008]. In the present study, aqueous photolysis of FPD is monitored in the presence of controlled and continuous UV-exposure. It is worth mentioning that the UV lamp is chosen over natural sunlight since an extremely slow change is observed in ^{1}H and ^{19}F NMR spectra of FPD when exposed to sunlight. Further, maintaining a controlled and continuous exposure of natural sunlight is difficult. Spectral changes in the case of ^{1}H NMR, as well as ^{19}F NMR recorded for FPD with UV exposure of 15 minutes to one hour, are found insignificant. However, UV radiation over a regular interval of approximately three hours period accomplished noteworthy changes in the ^{1}H and ^{19}F NMR spectra recorded in the absence of KHA. Figure 4.12 (a and b) exhibits the stack plot of ^{1}H and ^{19}F NMR resonances for UV exposed aqueous FPD solution in the absence of KHA recorded at various time intervals.

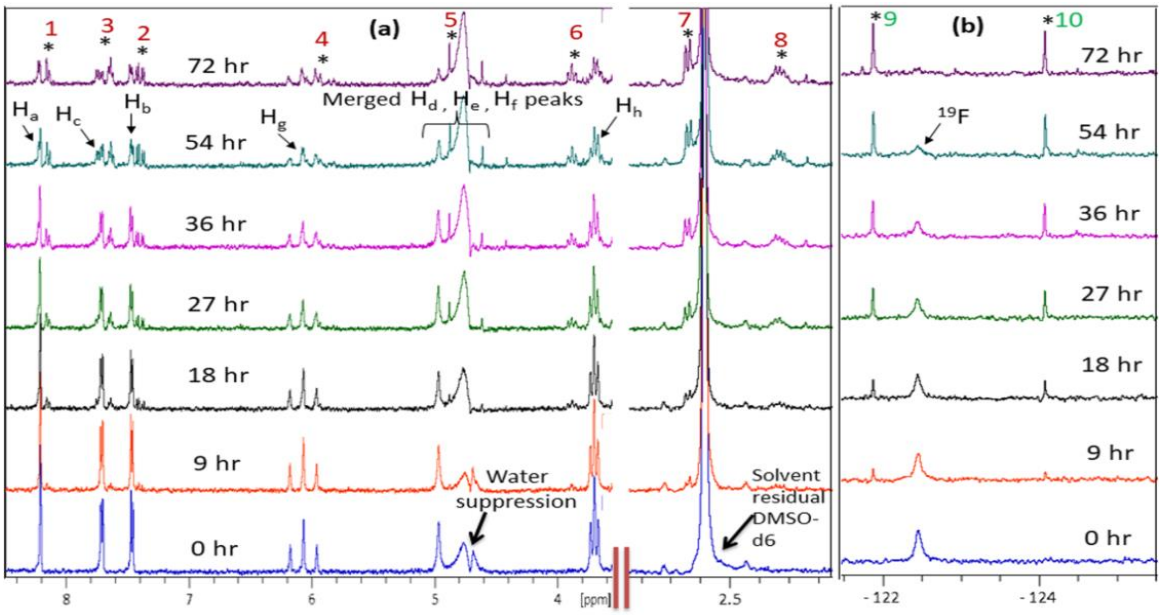

Figure 4.12: Photo-degradation of FPD prepared in 5: 95 DMSO: aqueous PB solvent system (pH=7.4) analysed by (a) ^{1}H NMR and (b) ^{19}F NMR as a function of time in the absence of KHA at 295 K. Arrows corresponding to H_a – H_h and ^{19}F represent the peak of parent FPD. Number *(1–10) describe the peak of formed photo-degraded products.

From the spectra shown in figure 4.12, a decrease in intensity of the resonances of FPD and increase in intensity of new peaks corresponding to degraded products (marked as *) can be seen as a function of time. The spectral intensities can be related to the concentrations of the parent molecule and the degraded products. Figure B7 given in Annexure B exhibits the several degradation products (designated as A–H) possible for FPD discussed in the literature [Flupyradifurone, 2013; Glaberman and Katrina, 2014]. Figure 4.13 explicitly represents the predicted degradation products in the current study based on ^{1}H NMR chemical shift values and peak patterns.

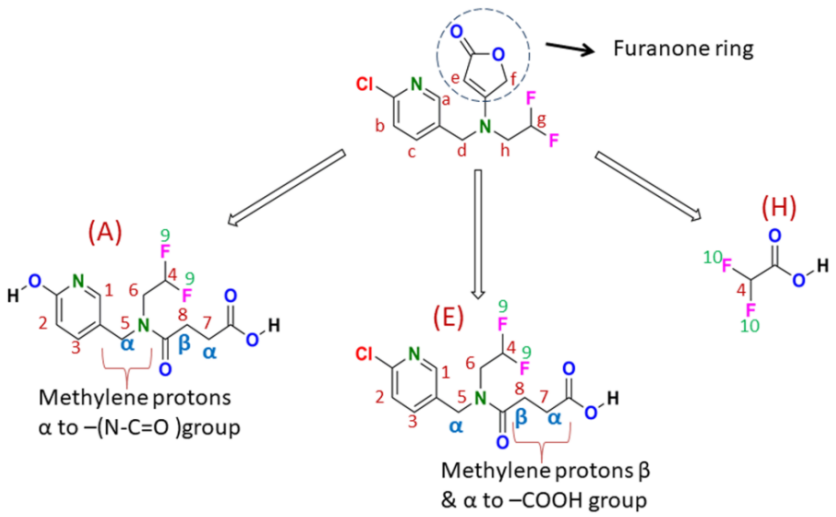

Figure 4.13: Scheme representing identified photo-degradation product in the present study for FPD prepared in 5: 95 DMSO: aqueous PB solvent system (pH=7.40) at 295 K. Here red numbers 1 to 8 indicate the relevant ^{1}H and green 9–10 numbers represent the ^{19}F NMR peak positions for the identified photo-degraded product of FPD shown on figure 4.12, 4.14 and 4.15 by (*).

A close inspection of Figure 4.12 revealed the following information related to the possible photo-degraded products appeared in the solution:
(i) Three new peaks marked as *1, *2, and *3 exhibiting similar coupling patterns as that of the existing FPD aromatic (pyridine ring) protons $-H_a$, $-H_b$, and $-H_c$ respectively have started appearing after 9 hours at upfield ppm positions. It demonstrates that a similar aromatic ring exists in the solution as one of the photo-degraded products; the upfield chemical drift is further representative of the distinct chemical environment of the newly formed chemical species compared to FPD (please refer to figure 4.13).
(ii) A triplet peak (marked as *4) upfield to $-H_g$ proton peak appears after 18 hours that matches with the ^{1}H NMR peak of DFA (compound H).
(iii) A new peak (marked as *5) has appeared in region 4.5 ppm – 5 ppm for the methylene protons alpha to –N–C=O (shown in figure 4.13).
(iv) Further, a new peak (marked as *6) of the same coupling pattern as $-H_h$ proton arises downfield to the $-H_h$ proton of FPD suggesting the presence of $-CH_2CF_2$ group (α to –N) similar to FPD in the aqueous photo-degraded products.
(v) Two new peaks are seen around 2.6 ppm (marked as *7) and 2.35 ppm (marked as *8) that can be respectively assigned to the methylene protons β and α to –COOH group formed only due to ring-opening of the furanone moiety of FPD (Please refer to FPD structure, FPD IUPAC nomenclature is 3-[(6-chloropyridin-3-yl)methyl-(2,2-difluoroethyl)amino]-2*H*-furan-5-one). These two peaks are indicative of the generation of compound A and E as degraded products due to ring-opening of furanone moiety (shown in figure 4.13).
(vi) Also, a new ^{19}F peak (marked as *9) arises downfield to the ^{19}F FPD resonance that can be assigned to the ^{19}F NMR peak of compound A and E whose ^{1}H NMR resonances have appeared in the upfield region of the ^{1}H NMR spectra of FPD marked as *7 and *8. These two observations undoubtedly confirm the possibility of aqueous photolytic conversion of FPD generating compound A and E.
(vii) Further, another sharp peak (marked as *10) has appeared in ^{19}F NMR spectrum upfield to the ^{19}F FPD resonance near –124.08 ppm that matched with the ^{19}F resonance for DFA confirming the formation of compound H (difluoroacetic acid, DFA) as one of the photo-degraded products.
(viii) On further irradiation of FPD continuously with UV source beyond 100 hours, all the peaks corresponding to the parent and the metabolites almost disappear in both ^{1}H and ^{19}F NMR spectra. It can be explained as the completion of the photolytic disintegration of FPD to carbon dioxide (CO_2) – one of the ultimate degradation products of FPD.

Hence, it can be said that the photochemical transformation of FPD proceeds via three main pathways; the rearrangement or ring opening of furnan-one (hydrolysis of the ester, photo-product A & E), photo-induced nucleophilic substitution of –Cl by –OH (photo-product A), and the cleavage through the aliphatic moiety followed by its oxidation (photo-product H).

Case (c)*:** As mentioned earlier, we are particularly interested to understand the possible effect of extracted HA (KHA, Karwar, India) on the photo-degradation of UV-exposed aqueous FPD (indirect photo-degradation). In line with the discussion of ***Case (a), KHA does not bring any change in the aqueous FPD NMR spectra recorded in the absence of UV irradiation except for inducing line broadening. These NMR experiments already recorded for aqueous FPD samples in the presence of KHA (0.2 and 2 mg/mL) and in the absence of UV irradiation for similar time intervals (-upto 4 days) are used as control (dark) experiments. The ^{1}H and ^{19}F NMR spectra do not show any change for these control samples. In contrast, the ^{1}H and ^{19}F NMR spectra of UV exposed FPD–KHA samples (figure 4.14 and 4.15) exhibit appearance and disappearance of similar spectral lines as for aqueous FPD solution irradiated with UV light in the absence of KHA suggesting the formation of same degradation products.

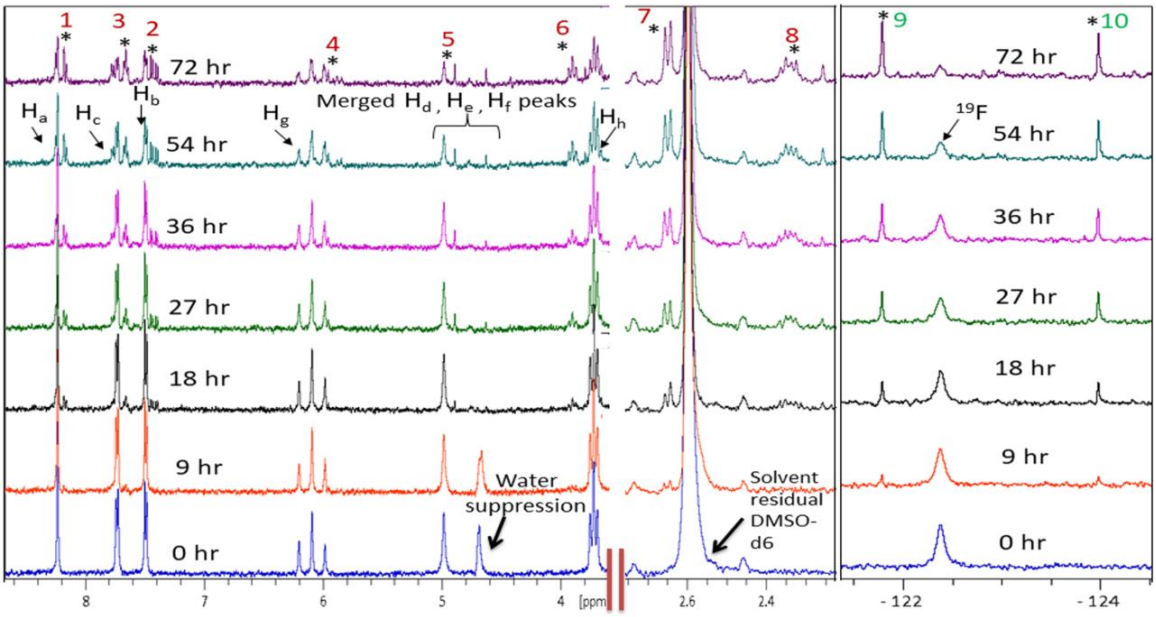

Figure 4.14: Photo-degradation of FPD in 5: 95 DMSO: aqueous PB solvent (pH=7.4) analysed by (a) ^{1}H NMR and (b) ^{19}F NMR as a function of time in presence of 0.2 mg/mL KHA at 295 K. Arrows corresponding to H_a – H_h & ^{19}F represent the peak of parent FPD. Number *(1–10) represents the peaks of formed photo-degraded products.

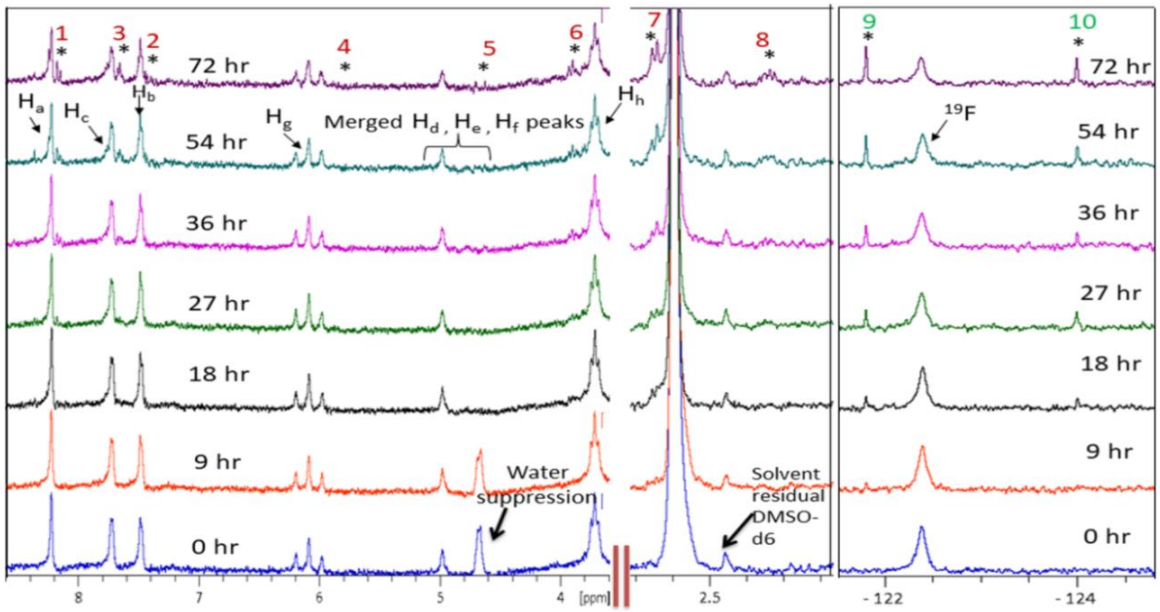

Figure 4.15: Photo-degradation of FPD in 5: 95 DMSO: aqueous PB solvent (pH=7.4) analysed by (a) ^{1}H NMR and (b) ^{19}F NMR as a function of time in presence of 2 mg/mL KHA at 295 K. Arrows corresponding to H_a – H_h & ^{19}F represent the peak of parent FPD. Number *(1–10) represents the peaks of formed photo-degraded products.

A closer analysis of figures 4.14 and 4.15 in terms of the appearance of new peaks as a function of time indicated different degradation kinetics for both the cases. The following section documents the quantification of the kinetics of photo-degradation in terms of rate constants and half-lives extracted by analysing the NMR spectral changes as a function of UV-exposure in the presence of KHA.

(c) Kinetics of FPD Photo-degradation in absence and presence of HA.

In order to evaluate the aqueous photolysis rate constant as well as the half-life of the process, all the ^{1}H and ^{19}F NMR peaks are integrated to calculate the percentage of FPD remaining at different time intervals of the measurement. The representative plot of experimentally measured integral values for H_b proton at 7.48 ppm, and the fluorine peak at −122.48 ppm against time is shown in figure 4.16.

The data are then fitted using equation 4.6 [Dahiya et al., 2020; Santoke et al., 2011], considering the photolysis process to be a pseudo-first-order reaction.

$$C = C_0 \exp(-k.t) \quad \text{.....(4.6)}$$

here, t is the UV irradiation time, C is the concentration of FPD at time t, C_0 is the initial concentration, and k in min^{-1} is the observed first-order rate constant of the reaction.

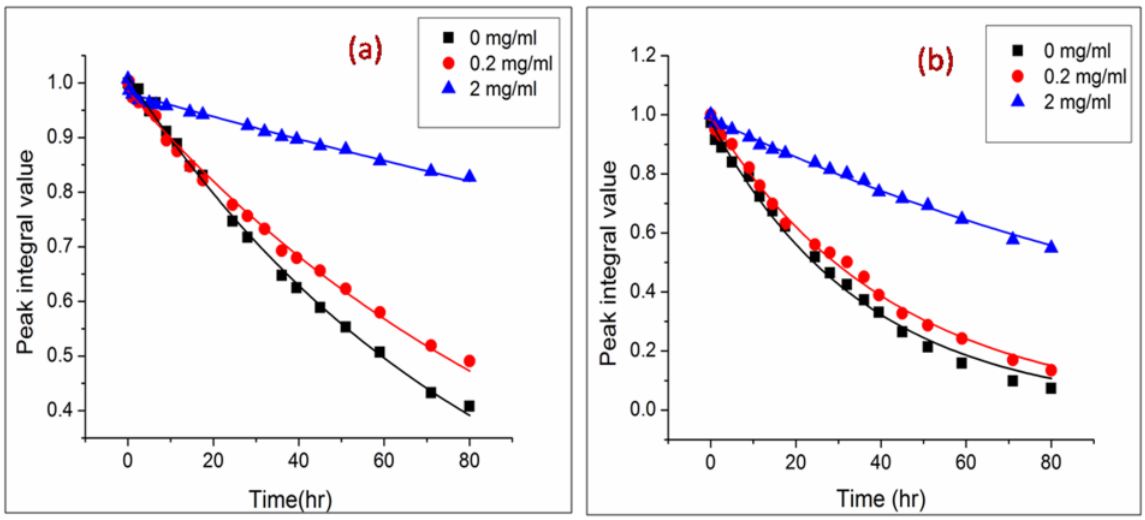

Figure 4.16: Representative plot of (a) ^{1}H (H_b) and (b) ^{19}F NMR peak integral values of FPD as a function of time with variable concentration of KHA (0, 0.2, and 2 mg/mL) prepared in 5: 95 DMSO: aqueous PB solvent (pH=7.4) measured at 295 K.

A preliminary analysis of figure 4.16 demonstrates that on the addition of KHA, the aqueous photo-degradation rate of FPD has significantly reduced. Interestingly, 0.2 mg/mL KHA is sufficient enough to retard the process effectively. A tenfold increase in KHA concentration (2 mg/mL) decreases the rate considerably, indicating the possibility of complete arrest of the degradation process at even higher concentrations of KHA. Table 4.5 summarizes the extracted average photo-degradation rate constants obtained from different protons of FPD and corresponding half-lives for FPD in the absence of KHA and presence of 0.2 mg/mL and 2 mg/mL KHA using both ^{1}H and ^{19}F peak integral values. In degradation processes of pollutants, half-life ($t_{1/2}=\ln 2/k$) is a parameter that accounts for the stability and persistence of a chemical substance in the environment. Here, it is defined as the time it takes for an amount of a compound to be reduced to half of its initial concentration through degradation.

Table 4.5: Observed average pseudo first order photo-degradation rate constant (k) and corresponding degradation half-life ($t_{1/2}$) for 1 mM FPD in absence and presence of 0.2 mg/mL and 2 mg/mL KHA prepared in 5: 95 DMSO-d_6:aqueous PB solvent (pH=7.4) at 295 K.

	^{1}H NMR			^{19}F NMR		
System	$k \times 10^{-4}$ (min^{-1})	$t_{1/2}$ (min)	R^2	$k \times 10^{-4}$ (min^{-1})	$t_{1/2}$ (min)	R^2
FPD + 0 mg/mL KHA	$^*k_d$ = 1.88 ± 0.04	3686.2	0.992	$^\#k_d$ = 4.61 ± 0.13	1503.2	0.993
FPD + 0.2 mg/mL KHA	$^*k_{id}$ = 1.42 ± 0.04	4880.3	0.986	$^\#k_{id}$ = 3.93 ± 0.07	1763.4	0.996
FPD + 2 mg/mL KHA	$^*k_{id}$ = 0.47 ± 0.02	14744.7	0.971	$^\#k_{id}$ = 1.19 ± 0.03	5823.5	0.992

k_d: denotes direct photo-degradation rate in absence of KHA; k_{id} : denotes indirect photo-degradation rate in presence of KHA; *: rate constants extracted using ^{1}H peak integral; #: rate constants extracted using ^{19}F peak integral data.

A close inspection of the table 4.5 reveals a number of interesting facts related to the aqueous photo-degradation of FPD. The most striking observation is made in terms of differential degradation rates measured from ^{1}H and ^{19}F peak integral data. The rate constant measured for aqueous FPD in the absence of KHA using ^{19}F peak integrals ($^\#k_d$) is *ca.* 2.5 times higher than the rate constant extracted from the ^{1}H peak integrals ($^*k_d$) measured for the same sample. Similarly, the half-life measured using ^{1}H data is 2.5 times higher than the half-life extracted using the ^{19}F data. This observation clearly indicates that the rate constants measured do not represent the global degradation process of FPD, rather a step-wise degradation of the molecule occurs in solution in absence of KHA. It can be recognized that the fluorinated aliphatic moiety of FPD disintegrates faster compared to the chlorinated pyridine ring. Due to the initial detachment of the fluorinated part, the overall chemical environment in terms of electron distribution changes that causes a shift in chemical shift values of the aromatic region, keeping the coupling pattern intact as discussed in previous section. It must be emphasized here that NMR is able to provide such subtle information regarding the steps of degradation of a molecule with certainty compared to the traditional UV-Vis spectroscopy. Further, analysis of the data presented in table 4.5 indicates that the aqueous direct photo-degradation rate constants (k_d) of FPD in the absence of KHA obtained from ^{1}H and ^{19}F spectra are around 25% and 76% faster than the rate constants (k_{id}) measured for FPD in the presence of 0.2 mg/mL and 2 mg/mL KHA respectively. A point to be noted here that a tenfold increase in KHA (2 mg/mL) concentration results in a threefold decrease in the rate constant (k_{id}) compared to that of 0.2 mg/mL of KHA indicating that the change of rate constant occurs disproportionately. Similarly, the corresponding half-life for FPD increases in the presence of KHA. Such alteration of the rate of degradation in the presence of KHA demonstrates that FPD and KHA undergo molecular association that alters the subsequent rate of degradation. The results undoubtedly prove that the presence of dissolved KHA heavily influences the aqueous photolysis of FPD.

The inhibited rates of FPD degradation in the presence of KHA demonstrate two aspects: i) KHA inhibit the UV radiation to reach the KHA bound FPD by trapping all the UV photons. KHA absorbs most of the UV photons available for degradation of FPD and thereby creating an effect known as an optical filter or light screening that leads to slowing down of photochemical degradation of FPD [Arias-Estévez et al., 2008; Goring et al., 1975]; ii) FPD might be partially bound to or encapsulated by KHA through the chlorinated pyridine ring that prevents the •OH to impart photolysis action [Si et al., 2004]. The generated •OH radical in the aqueous solution are not able to come in direct contact of encapsulated FPD (due to host-guest types interaction between FPD and HA) and oxidise them to generate the degradation products.

The excited states of agrochemicals generated via the direct absorption of light are known to be quenched by dissolved organic matter present in natural waters [Katagi, 2018]. Hence, it can be anticipated that in presence of KHA, these excited chemical molecules are deactivated by the energy-transfer and charge-transfer between the FPD and HA and thereby causing the photo-quenching effect for KHA encapsulated FPD. The differential degradation rate constants extracted from ^{19}F peak integral data could possibly indicate the higher accessibility of fluorine moiety towards •OH radical and the plausible binding mode of FPD to KHA. One may anticipate that FPD binds to KHA or enters KHA micellar superstructure through the chlorinated pyridine ring while the fluorinated aliphatic region prefers to remain outside the cavity that allows •OH radical to initiate the photolysis of the fluorinated moiety resulting in faster disintegration. As an overall effect, the encapsulation process inhibits the degradation process. Figure 4.17 represents the summary of the overall findings of the current photo-degradation study and the mechanism involved. To the best of our knowledge, the aqueous photo-degradation of FPD in the presence of a HA under laboratory conditions has been studied for the first time employing NMR.

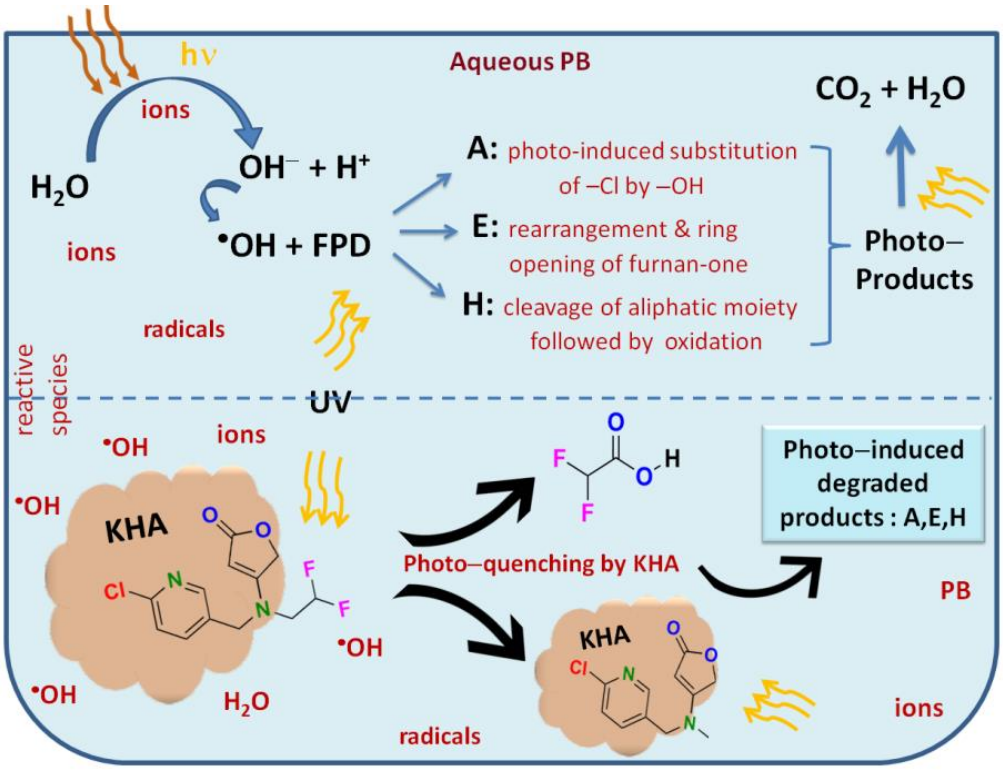

Figure 4.17: Graphical representation of the expected plausible mechanism for the photo-degradation of UV exposed FPD in the absence (top trace) and presence (bottom trace) of KHA in aqueous phosphate buffer (PB). A, E, H are the identified possible photo-degraded products whose structure is given in figure 4.13. (Plausible mechanism for degradation of free FPD has been discussed briefly in section B3: Annexure B).

Naturally, the next aim of the present study is to quantify the association of FPD with KHA, followed by detecting the possible binding mode of FPD to KHA. DFA appears as one of the major photolytic degraded product for FPD. Hence, it is meaningful to compare the binding efficacy of FPD-KHA with that of DFA–KHA to further comment on the fate of FPD in soil-water system as discussed in the following sections.

(ii) Molecular interaction of FPD with KHA: Application of NMR relaxation, diffusion and magnetization transfer based measurements

In the following, we have attempted to use NMR relaxation for providing qualitative and diffusion measurements for extracting quantitative details of FPD–KHA and DFA–KHA interactions in aqueous media. Further, chemical shift and STD NMR analysis are carried out to shed light on the binding mode of FPD and DFA while interacting with KHA.

(a) Qualitative evaluation of KHA binding using FPD and DFA ^{1}H and ^{19}F relaxation rates

Both ^{1}H and ^{19}F T_1 and T_2 measured for FPD and DFA (the spectral analysis of DFA, product H shown in figure 4.13 is provided in table 4.4) are found to be decreasing with increase in KHA concentration. It is a well-known fact that the ratio of T_1/T_2 varies as a function of molecular correlation time (τ_c) in solution and can perfectly reflect whether a molecule moves from one motional regime to another due to molecular aggregation or interaction; in particular for a small molecule experiencing fast motion in solution, the magnitude of T_1/T_2 is nearly unity while for a supramolecule / macromolecule the ratio deviates far beyond unity [D'Agostino et al., 2014]. In the present case, figure 4.18 (a & b) represents the T_1/T_2 ratio (^{1}H and ^{19}F) as a function of KHA concentration for both FPD and DFA molecules.

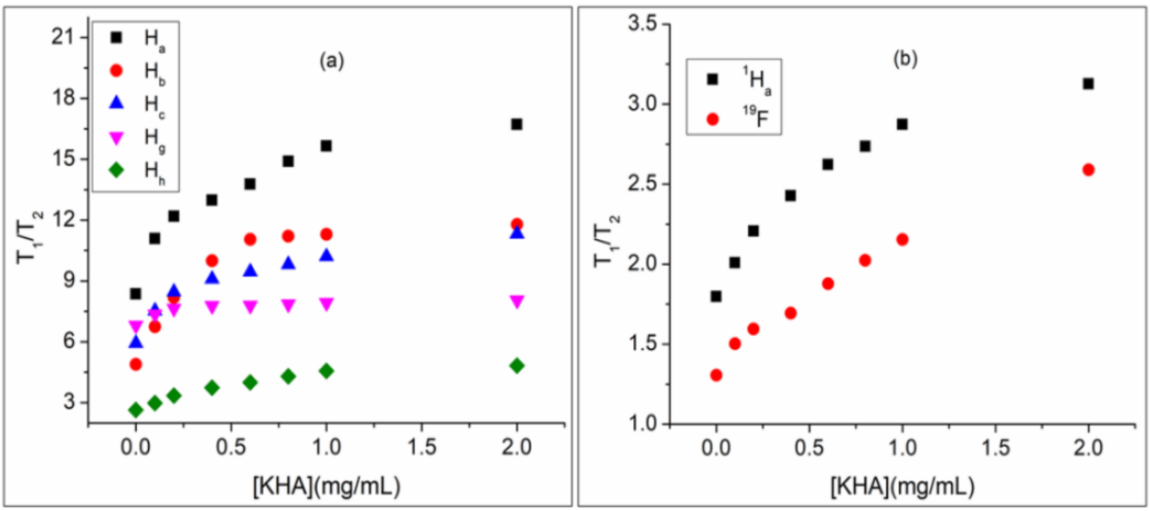

Figure 4.18: Plot of ^{1}H and ^{19}F NMR relaxation ratio (T_1/T_2) for (a) FPD and (b) DFA prepared in 5: 95 DMSO: aqueous PB (pH=7.40) as a function of KHA concentration measured at 295 K.

The corresponding values of T_1/T_2 ratio (^{1}H and ^{19}F) for each proton and –F of FPD and DFA are reported in table B5 (Annexure B). It is clearly seen figure 4.18 and table B5 (Annexure B) that T_1/T_2 ratio changes significantly for all the protons compared to the fluorine T_1/T_2 in the case of FPD. Further, among the protons, the chlorinated pyridine ring protons exhibit a considerably greater change in the T_1/T_2 as a function of KHA concentration compared to the T_1/T_2 ratio observed for the fluorinated aliphatic moiety protons. This observation undoubtedly points out that FPD interacts with KHA; more specifically, FPD enters the KHA superstructure cavity from the chlorinated aromatic (pyridine) ring side while the fluorinated aliphatic moiety remains outside of the cavity. Such an encapsulation process imparts differential motional behaviour to the various protons. On the other hand, ^{19}F T_1/T_2 ratios in the case of FPD do not exhibit marked changes in the absence and presence of KHA. Moreover, for DFA, the changes observed for the aliphatic proton and ^{19}F T_1/T_2 ratio in the absence and presence of KHA are also nominal, indicating that DFA encapsulation by KHA is not as effective as that of FPD. In the case of FPD, T_1/T_2 for all the protons increases progressively and reaches a plateau beyond 1 mg/mL KHA

concentration, probably indicating saturation of the encapsulation process. While in case of DFA however, the T_1/T_2 ratio does not seem to reach a plateau indicating possibility of further encapsulation of DFA in the presence of KHA beyond 2 mg/mL concentration [Nanny and Maza, 2001; Šmejkalová and Piccolo, 2008b; Šmejkalová et al., 2009]. ^{19}F T_1/T_2 ratio for DFA showed maximum increase from 1.3 to 2.6 (~ 50% increase). On the other hand, the change in ^{19}F T_1/T_2 ratio for FPD (50.58 to 61) are of lower extent *i.e.* 17% increase in the ratio. This observation suggests that –F moiety of FPD may not be involved in the interaction event.

(b) Quantitative evaluation of binding through Diffusion measurement:

In this section, self-diffusion coefficients of FPD and DFA are measured in the absence and presence of variable KHA concentrations at 295 K and pH 7.4. Table B6 (Annexure B) compared the experimentally measured self-diffusion coefficient (D) values of FPD and DFA as a function of KHA concentration. A marked decrease in the viscosity corrected D values from 4% to 40% in the case of FPD and from 3.5% to 25% in the case of DFA is observed with increasing concentration of KHA. The attenuation in D values can be attributed to the fact that FPD and DFA interact with KHA superstructure through weak non-covalent interaction due to which both the test molecules experience a change in their mobility in solution. The test molecules attain the supramolecular behaviour of slow molecular motion in solution on encapsulation by KHA superstructure [Longstaffe et al., 2016]. It must be pointed out that the experimentally measured D values for both FPD and DFA in presence of a specific KHA concentration are average of the free and encapsulated state diffusion coefficients of the test molecules. The change in D values is dependent on the equilibrium between free and the encapsulated test molecules. In the present case the reported D values are viscosity corrected [Wimmer et al., 2002]. These corrected D values are then used to extract the r_H values of FPD and DFA in the absence and presence of KHA and are found to be increasing with increasing KHA concentration. The bound fraction for FPD and DFA are calculated from their ^1H D values employing equation 2.21, chapter 2, since the ^{19}F peak observed for FPD in the presence of KHA becomes extremely broad that hinders meaningful measurement of peak integral required for extraction of D values.

Figure 4.19 represents the P_b values (reported in table B6: Annexure B2) calculated for FPD and DFA plotted against increasing concentration of KHA (mg/mL).

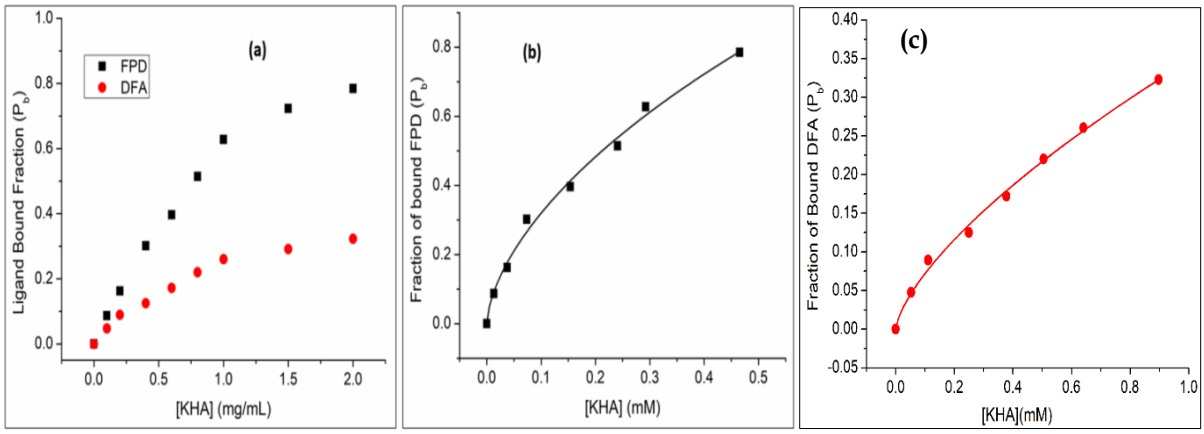

Figure 4.19: (a) Plot of bound fraction calculated from D values for FPD and DFA against KHA concentration. Plot for determination of K_A for (b) FPD–KHA and (c) DFA–KHA prepared in 5: 95 DMSO: aqueous PB (pH=7.40) at 295 K using P_b values calculated from respective ^1H D values against KHA concentration. Symbols (square and circle) represent the data points. Solid lines are obtained by fitting through the modified Langmuir model.

The plot exhibits the higher tendency of FPD (significantly higher bound fraction at highest KHA concentration) to be encapsulated by KHA compared to that of DFA. Further, the association constant (K_A) for each system has been determined to compare the strength and stability of the host-guest complex formed between KHA and the test molecules [Šmejkalová et al., 2009] by fitting the test molecule bound fractions against KHA concentration (mM) by employing modified Langmuir model considering wide heterogeneity of binding domains of humic superstructures available for encapsulation. Figure 4.19 (b) represent the fitted bound fraction against KHA concentration for FPD while a similar plot for DFA is provided in figure 4.19 (c). Relevant discussion on modified Langmuir model fitting has been discussed in previous section Part I-4.3.1 (d). Furthermore, the K_A values extracted form figure 4.19 (b) and (c) allow the calculation of $\Delta G°$ for the interaction of host-guest complex formed are reported in table 4.6.

Table 4.6: Binding constant (K_A) and Gibbs free energy of transfer ($\Delta G°$) for the association of FPD–KHA complex and DFA–KHA complex at 295 K and pH=7.40.

System	K_A (M^{-1})	R^2	ln K_A	$\Delta G°$ (kJ/mol)
FPD–KHA	55.55±7.40	0.992	4.02	−9.83
DFA–KHA	10.90±2.32	0.991	2.39	−5.84

*Errors mentioned for K_A are average standard deviations calculated from independent experiments

A close inspection of table 4.6 reveals that the association of FPD within KHA superstructures is *ca.* 5 times stronger than the DFA–KHA host-guest complex. The negative values of $\Delta G°$ for both the system confirm that the encapsulation of FPD and DFA to KHA superstructure is a spontaneous process and thermodynamically favourable. Further, in the following section the mode of insertion of FPD and DFA within KHA superstructure has been analysed employing chemical shift changes and STD NMR data recorded for FPD–KHA and DFA–KHA.

(c) Evaluation of Binding mode by chemical shift and STD NMR measurements:

^1H and ^{19}F NMR peaks of FPD have been monitored in the presence and absence of different KHA concentrations as discussed in section 4.3.2 i(a). The changes in chemical shifts of FPD on the addition of KHA in the solution are indicative of molecular interaction between FPD and KHA. ^1H–^1H and ^1H–^{19}F STD NMR experiments have allowed GEM that further pave the path of identifying the chemical groups of FPD in spatial proximity with KHA chemical moieties during the interaction. The major outcomes are: a) the drift in ^1H chemical shifts observed for FPD (figure 4.11 and figure B6: Annexure B) is of variable extent for different protons exhibiting maximum upfield drift of 7.93 Hz for $-H_b$ proton in the aromatic (pyridine) moiety in presence of the highest KHA concentration; b) the ^{19}F NMR showed a maximum downfield shift of 6.13 Hz for the same KHA concentration; c) ^1H–^1H STD measurements indicated highest saturation transfer for the protons situated in the chlorine substituted aromatic ring; d) ^1H–^{19}F STD NMR does not exhibit any detectable saturation transfer for the ^{19}F peak of FPD. The observations regarding changes in the chemical shifts can be reasoned out as follows: i) In accordance to the literature the upfield shifts of ^1H chemical shifts indicate formation of halogen-bonds between chlorine substituents of the test molecule and complementary groups in KHA [Beer et al., 1989; Šmejkalová and Piccolo, 2008b]. Also, possibility of π–π interactions between FPD aromatic ring and KHA aromatic substituents results of an increased electron shielding around the proton nuclei situated in the aromatic ring of FPD [Veil et al., 2002]; ii) the observed downfield shift in ^{19}F resonance occurs due to reduced electron shielding around –F nucleus as a result of a non-fluorine group of a nonionic organic molecule being involved in interaction with HS [Chelli et al., 2007; Dixon et al., 1999; Herbert and Bertsch, 1997]. The observed chemical shift changes in

^{1}H and ^{19}F resonances indicates that KHA superstructure in solution encapsulates FPD perhaps in its hydrophobic domain through non-covalent interactions. Such encapsulation by hydrophobic domain either governed by halogen bonding or π–π interactions may reduce the solvent-fluorine interaction resulting in downfield shift of ^{19}F resonances for the test molecule [Chelli et al., 2007; Herbert and Bertsch, 1997; Šmejkalová et al., 2009]. GEM for FPD as unravelled from the STD measurements enables the identification of parts of FPD spatially proximal to KHA during the interaction [Angulo et al., 2010; Cala and Krimm, 2015].

Figure 4.20 represents the ^{1}H–^{1}H STD spectrum for FPD–KHA. The relative percentage STD values (R_{STD} (%)) for FPD protons obtained on the basis of peak integral values are reported in figure 4.20 confirming that the pyridine ring protons (H_a, H_b, H_c) of FPD are in close proximity with KHA protons. The –H_b proton near the chlorine substituent receiving 100% saturation suggests that FPD enters the hydrophobic cavity of KHA superstructures through the chlorine substituted pyridine ring side. ^{19}F observed ^{1}H–^{19}F STD experiment shows no detectable signal intensity in the STD_{diff} spectrum for FPD (figure not shown). It is well known that among the halogens –Cl shows better interaction through halogen bonding compared to –F [Gilday et al., 2015]. It can, therefore, be inferred that the chlorinated pyridine ring is more prone to enter the KHA cavity than the aliphatic moiety containing –F (–CHF_2) further confirming that the fluorinated chemical moiety of FPD remains far from the KHA cavity (as evident from ^{1}H–^{19}F STD experiments). This observation matches well with the literature that discussed a stronger binding of chlorinated phenol with HA than fluorinated one [Šmejkalová et al., 2009]. This is also in agreement with the findings of photo-degradation kinetics that confirmed slow photolytic degradation of the chlorinated aromatic ring compared to that of the furanone ring and fluorine moiety that receives better UV exposure by remaining outside the KHA domains. Similar STD analysis for DFA is presented in Annexure B as section B4 that depicts that –F of DFA interacts with KHA.

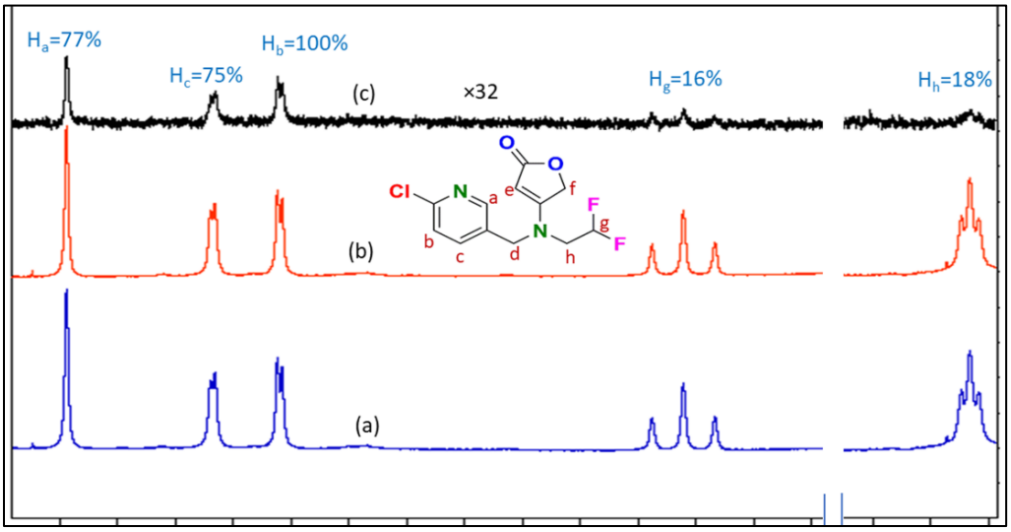

Figure 4.20: ^{1}H–^{1}H NMR (a) STD_{off} (b) STD_{on} and (c) STD_{diff} spectrum for FPD–KHA system prepared in 5: 95 DMSO: aqueous PB solvent (pH=7.4) and measured at 295 K.

A point to be noted here is that the humic structure investigated could not be visualized as "static" since the properties and structure of HA are highly dependent on the source and its genesis. Therefore, the obtained results are particularly true for the effect of KHA on FPD and

hence should not be taken as granted and reproducible with any other HA extracted from different soil samples or aquatic media.

4.4 CONCLUSIONS:

The present analysis summarizes the structure and molecular interaction of two types of HA, one commercially obtained peat/ lignite coal humic acid (AHA) and another extracted (KHA) from field soil of the western part of Rajasthan (arid region), India with organic molecules employing solution-state NMR methods. It has been realized that both structural and interactional complexity of HA demand application of a range of multiphasic analytical techniques to unveil interaction of HA at the molecular level. Solution-state 1D ^{1}H and ^{19}F NMR methods provide a comprehensive analysis of HA-pollutant interaction. Chemical shift, and relaxation analysis gives clear evidence that all the molecules investigated in both parts of current study (*viz*., DFBA, BA, FPD and DFA) bind significantly to respective HA through non-covalent interactions at neutral pH conditions. Therefore, these complexes may have potential to move through soil profiles and pollute water bodies. STD NMR analysis confirmed that the mode of interaction of organic compounds with HA majorly depends on the functional groups present in the molecule. On the other hand, NMR diffusion measurements quantified the molecular association in terms of association constants and Gibbs free energy change indicative of a spontaneous encapsulation process for all the investigated molecular systems.

In part I, it is found that carboxylic acid group plays a vital role in the binding mechanism of BA with HA, while in the case of –F substituted BA (DFBA), –COOH group is oriented away from the HA during the interaction. Further, it is also found that the substitution of –H with halogen –F increases the binding strength of CA–HA complexes. The stronger binding strength of DFBA–AHA suggests that AHA can serve as a potential remediating agent for DFBA contaminated soil and water. The present study also indicates that the source and genesis of HA play a vital role in influencing the extent of association of these organic CAs towards HA; in specific the more humified AHA acts as a better binder to DFBA than the less humified KHA. It might be interpreted that CA binds through the lignin component present majorly in AHA. While in the case of KHA, the presence of other natural chemical components, namely proteins, carbohydrates, peptides, cuticular materials in addition to the lignin causes limited accessibility of lignin binding sites for DFBA. Therefore, it could be envisaged that soil from arid region will not retain DFBA due to the presence of less humified HA. Furthermore, the DFBA–HA molecular interaction has potential to be extrapolated to analyse interaction between HA extracted from various regions and large fluorinated carboxylic acid molecules that are insoluble in aqueous media and are either prepared from or degrade to DFBA.

In part II, KHA significantly quenches the aqueous photo-degradation rate of FPD, indicating light screening property of KHA. All the photo-degradation processes (for free FPD and FPD–HA systems) followed similar pseudo first-order chemical kinetics and generated the same degradation products under all experimental conditions. The extracted photo-degradation rates and corresponding half-lives are useful parameters for assessing the persistence of FPD in soil-water systems. Superior rates found for FPD in the presence and absence of KHA using ^{19}F NMR data compared to that of the ^{1}H NMR data demonstrated that FPD undergoes stepwise disintegration where the fluorinated aliphatic moiety leaves the molecule first. Interestingly, STD GEM also revealed that the fluorinated aliphatic moiety does not participate in molecular association with KHA while the chlorinated aromatic region possibly enters the cavity of the KHA superstructure. It is thereby justifiable to anticipate that such molecular encapsulation of the aromatic moiety by KHA prevents it from absorbing UV photons required for photo-degradation while the fluorinated aliphatic moieties receive enough UV photons that initiate the detachment process. Molecular association between FPD and KHA is confirmed using relaxation analysis that undoubtedly indicated FPD moving from small molecule motional

regime in solution to macromolecular motional regime in presence of KHA. Such molecular association can be considered to be host-guest interaction where FPD behaves as a guest and KHA plays the role of a host and occurs through halogen bonding via the chlorine substituent of the aromatic moiety of FPD. Further, our results clearly demonstrated that DFA-KHA association is weaker compared to that of FPD–KHA and would, therefore, allow DFA (more mobile) to leach out to groundwater or surface water more quickly compared to that of FPD. At the same time, FPD will remain on soil for a longer time.

….